

36 and contribution to sea level, especially given that more of these extremes are predicted under a
37 warmer climate.

38 **Keywords:** Ice shelf calving, icebergs, Amery Ice Shelf, East Antarctica, blocking highs, polar
39 cyclones, explosive cyclones.

40 1. Introduction

41 The rapid collapse of several Antarctic ice shelves, observed recently, and the near-instantaneous
42 acceleration of land-ice discharge into the ocean that follows the collapse, demonstrates the
43 sensitivity of the Antarctic cryosphere to recent warming (e.g., Smith et al., 2019; Rignot et al.,
44 2019). However, large uncertainty remains regarding the response of ice shelves to the globally
45 rising temperatures and to the resulting changes in the atmospheric circulation.

46 On 25 September 2019, the Amery Ice Shelf – the third largest ice shelf in Antarctica – calved
47 iceberg D28 (1,636 km², 210 m thick), which was the largest calving event since the early 1960s
48 (Fig. 1). The Amery Ice Shelf is a key drainage channel in East Antarctica (Fricker et al., 2002)
49 draining roughly 16% of the East Antarctic Ice Sheet (Galton-Fenzi et al., 2012). It is ~~considered~~
50 in balance with its surroundings (King et al., 2009; Galton-Fenzi et al., 2012; [Li et al., 2020](#)),
51 despite experiencing strong surface melt in summer. However, over the past 20 years, a large
52 system of rifts (a precursor to calving) in the Amery Ice Shelf, known as the Loose Tooth rift
53 system, has been developing (Fricker et al., 2005; Bassis et al., 2008; [Darji et al., 2018](#)). Recent
54 studies have shown that the propagation rate of the rifts has been decreasing since 2005 due to
55 increasing thickness of mélange ice filling in the rifts, and speculated that forward propagation of
56 the west rift might even stop (e.g., Zhao et al., 2013). Satellite images of the Amery Ice Shelf (Fig.
57 1) show the largest rift extending in the same direction of the ice flow, widening toward the edge
58 of the ice shelf and from this main rift, with radial rifts extending to the west (T1) and east (T2).
59 Earlier studies predicted that the Amery Ice Shelf ~~would not experience a major calving until~~
60 ~~around 2025 or later. would not experience a major calve until at least 2025 or later~~ (e.g., Fricker
61 et al., 2002), and the portion that was expected to calve first was T2 i.e., the one to the east of the
62 current calving. This highlights the need for an improved understanding of the underlying
63 processes of calving events and the role of atmospheric forcing ~~as trigger for in-ice shelf calving.~~
64 ~~weakening; a precursor to rapid and major changes in ice shelf stability.~~

65 Indeed, most of the mass loss from the Antarctic Ice Sheet – the largest uncertainty for future sea
66 level projections – takes place at the fronts of ice shelves and glacier tongues, via iceberg calving
67 and surface and basal melt (e.g., Pritchard et al., 2012; Shepherd et al., 2018). Compared to
68 melting, rifting and subsequent calving is the fastest way by which marine-terminating glaciers
69 lose mass to the ocean and contribute therefore to sea level rise (e.g., Smith et al., 2019). Despite
70 being floating ice (i.e., changes in their mass due to calving do not have a direct contribution to
71 sea level rise), ice shelves ~~in general~~ act to buttress inland ice by blocking the flow of ice from the
72 interior ([Scambos et al., 2008](#)). This restrictive force decreases when ice shelves thin or calve.
73 ~~Calving from floating ice shelves contributes indirectly to sea level rise as these events accelerate~~
74 ~~the rate of ice flow from grounded ice sheet into the ocean (e.g., Hogg and Gudmundsson, 2017).~~
75 For example, on the Antarctic Peninsula, such events have been shown to increase by eight-fold

76 the rate of ice flow inland (Rignot et al., 2004; Scambos et al., 2004; [2014](#)). This leads to more ice
77 discharge into the oceans and a consequent increase in the ice-sheet contribution to global sea-
78 level rise (Hogg and Gudmundsson, 2017). Ocean-driven thinning was also detected at key ice
79 shelves of the East Antarctic Ice Sheet including the Amery Ice Shelf (Greenbaum et al., 2015;
80 Smith et al., 2019) suggesting that this region is also susceptible to rapid and large-scale ice loss
81 (Aitken et al., 2016), and could contribute to future sea-level rise (DeConto et al., 2016; Rignot et
82 al., 2019). Therefore, there is a ~~n-urgent~~ need to assess the sensitivity of East Antarctic ice shelves
83 to atmospheric forcing and to understand the calving processes governing processes and their
84 triggers in order to be able to model the future evolution of ice shelves.

85 Beyond being part of a natural glaciological process, calving events at Antarctic ice shelves have
86 been attracting much attention recently (e.g., Liu et al., 2015; Benn and Astrom 2018) as they were
87 found to trigger, in some cases, the total disintegration of the parent ice shelf (Cook and Vaughan
88 2010; Liu et al., 2015; Jeong et al., 2016; Bassis and Ma, 2016; Massom et al., 2018). These events
89 have been attributed mainly to an enhanced regional warming (Vaughan et al., 2012; Pitchard et
90 al. 2012) which increases surface and basal melt as well as to ocean forcing involving intense
91 crevassing and rifting along multiple lines of weakness such as radial crevasses (Liu et al., 2015;
92 Jeong et al., 2016; Bassis and Ma, 2016), -to earthquake and tsunami (Brunt et al., 2011) and to
93 regional loss of pack ice in the shelf-front area which allows storm-generated ocean swell to flex
94 the outer margins of the shelves and lead to their calving (Massom et al., 2018). However,
95 atmospheric-dynamics forcing during ~~such calving~~ events, particularly the wind mechanical action
96 on rift widening ~~both directly and via wind-induced~~ tides and ocean slope waves, remains
97 unexplored and this the objective of this study.

98 ~~Despite the importance and the implications of ice shelf calving, this phenomenon remains~~
99 ~~unpredictable and is still poorly understood. Moreover, the underlying mechanisms governing~~
100 ~~Antarctic ice shelf instability, especially those associated with atmospheric extremes, remains~~
101 ~~unknown.~~

102 Of particular importance is the impact on Antarctic ice shelves of the poleward shift of
103 extratropical storm tracks (Tamarin and Kaspi, 2017) and the observed increase in the number and
104 intensity of cyclones around Antarctica over the last few decades ([Rudeva et al., 2015](#); Wei and
105 Qin 2016). The poleward shift of extratropical cyclones was found in reanalysis data of recent
106 years (Fyfe, 2003; Son et al., 2008), and models ([e.g., Neu et al., 2013](#)) project an estimated
107 poleward shift of cyclone genesis 1° to 2° in latitude on average under enhanced greenhouse gas
108 concentrations (Bengtsson et al., 2009; Barnes and Polvani, 2013). Importantly, this poleward shift
109 was found to be particularly pronounced in the Southern Hemisphere ([Pezza et al., 2007](#); Chang
110 et al., 2012), and the mean intensity of cyclones as well as the number of extreme cyclones are
111 projected to increase under a warmer climate scenario (Lambert and Fyfe, 2006; [Ulbrich et al.,](#)
112 [2013](#); Chang, 2017; [Kossin et al., 2020](#)).

113 Changes in cyclone tracks, numbers, and intensity may have significant impacts on Antarctic sea
114 ice and land ice ([e.g., Uotila et al., 2011](#)). In fact, weather systems (i.e., cyclones and blocks)
115 resulting from the larger-scale circulation (e.g., Pope et al., 2017) are identified as the main driver
116 of the observed trends in sea ice variability (Matear et al., 2015; Schemm, 2018; Turner et al.,

117 2017; Eayrs et al., 2019). Furthermore, cyclones and their associated atmospheric rivers can induce
118 sea ice melt (Francis et al., 2020) and ice-shelf surface melt (Wille et al., 2019) by virtue of their
119 associated -anomalous moisture and heat transport to high latitudes which increase the downward
120 longwave radiation at the ice surface (Woods & Caballero, 2016; Lee et al., 2017; Grieger et al.,
121 2018; Francis et al., 2020). Additionally, cyclones can cause significant sea ice drift (Kwok et al.,
122 2017; Francis et al., 2019a) due to the strong surface winds they carry (Schemm, 2018). Severe
123 storms can generate energetic waves (up to 8 m) in the Southern Ocean capable of penetrating
124 hundreds of kilometers into the sea ice covered ocean (Kohout et al., 2014; Vichi et al., 2019;
125 [Squire, 2020](#)). Concomitantly, the sea ice cover acts as a buffer and attenuates the wave energy
126 over distance ([wave amplitude is reduced by several orders of magnitude within 10km of the sea](#)
127 [ice edge](#)), reducing therefore the impact of storms on ice shelves (Dolatshah et al., 2018; Massom
128 et al., 2018).

129 An extreme situation in cyclogenesis is the formation of explosive cyclones. These are developing
130 cyclones for which the central pressure decreases by at least 24 hPa in 24 hours (Sanders and
131 Gyakum, 1980). Explosively developing cyclones are deeper and longer-lasting compared to
132 ordinary cyclones and they are found to be more intense in the Southern Hemisphere than in the
133 Northern Hemisphere (Raele et al., 2019). In particular, explosive cyclones in the Indian Ocean
134 sector of the Southern Ocean (close to South Africa) are stronger and express higher deepening
135 rates than elsewhere around Antarctica (Raele et al., 2019). This same region (between 45°E and
136 90°E and poleward of 40°S) – encompassing the Amery Basin – stands out in a climatological
137 study (Allen et al., 2010) as one of three main regions for explosive cyclogenesis around
138 Antarctica, where explosive cyclones are characterized by a 20hPa mean pressure depth relative
139 to the surrounding pressure field. A climatological study of explosive cyclones (Lim and
140 Simmonds, 2002) found that the number of explosive cyclones increased in both hemispheres
141 during 1979-1999, and that positive trends of such systems are statistically significant in the
142 Southern Hemisphere. On average, the study identified 26 explosive cyclones per year in the
143 Southern Hemisphere and found that explosive cyclones exhibit greater mean intensity and depth
144 relative to the entire population of ordinary cyclonic systems. A more recent climatological study
145 over a longer period (1979–2013) reported similar findings, with an increase in the frequency of
146 explosive cyclones in the band of 45°–55°S during winter and early spring (Wei and Qin 2016).

147 The spatial distribution of these cyclones was found to have a close association with that of strong
148 baroclinicity. In general, the preferred region for cyclogenesis is where both a strong temperature
149 gradient and an upper-level trough are present (e.g., Shimada et al., 2014). While high baroclinic
150 instability associated with the horizontal temperature gradient is crucial for the formation and the
151 intensification of cyclones (Davies, 1997, Uccellini, 1990), cyclogenesis occurs only at the
152 entrance and exit regions of upper-level troughs (e.g., Shimada et al., 2014). Around Antarctica,
153 the strongest temperature gradient is found during late winter-early spring along the fringes of the
154 ice pack, making the sea-ice edge a preferred region for cyclogenesis (e.g., Schlosser et al., 2011;
155 Stoll et al., 2018). However, the location of the temperature gradient relative to the ice edge
156 depends strongly on the atmospheric circulation at larger scale, where a strong temperature
157 gradient can occur poleward of the ice edge (i.e., closer to the ice shelves) during an enhanced
158 zonal wave number three (ZW3) pattern ([Irving and Simmonds, 2015](#)~~Francis et al., 2019~~). This

159 pattern is characterized by the alternation of 3 troughs and 3 ridges around Antarctica. Strong
160 poleward transport of heat and moisture occurs in the ascending branch of troughs and strong
161 equatorward transport of cold air occurs in the descending branch of ridges (e.g., Raphael, 2007).
162 This zonally-alternating pattern of cold and warm air masses creates temperature differences
163 between the different sectors, fuels frontogenesis and promotes the development of explosive
164 cyclones close to the ice shelves and over the sea ice cover.

165 Another aspect of the ZW3 pattern is the impact of the ridges on the propagation speed of the
166 cyclones. In the troughs, the extratropical cyclones and the associated moisture and heat fluxes are
167 directed poleward; once they reach the Antarctic coast they are blocked by the ridges to their east
168 (Francis et al., 2019a; 2020). This results in stationary cyclones over the same region for 1-2 days
169 which in turn induces pronounced impact on the sea ice (e.g., Francis et al., 2019a) and waves
170 (Vichi et al., 2019). The same scenario can happen at the front of ice shelves during winter-spring
171 if the cyclones form closer to the coast and/or the sea ice extent decreases under a warmer climate.
172 Interestingly, the Antarctic sea ice extent has been decreasing since 2015 (Swart et al., 2018) and
173 the ZW3 index has been the most positive on record during the same period (Schlosser et al., 2018;
174 Francis et al., 2019a). Increased warm air advection toward Antarctica was found to be at the origin
175 of the observed negative anomaly in Antarctic sea ice extent in recent years (Schlosser et al., 2018).
176 Given the dual impact of ZW3 circulation on both explosive cyclogenesis (location and intensity)
177 and sea ice extent, this combination may result in a more pronounced impact of extreme cyclones
178 on ice shelves.

179 Another extreme situation in cyclogenesis is the formation of twin cyclones during which the
180 resulting effect of the mutually-interacting cyclones is twice as strong as the individual cyclones
181 (e.g., Moustouli et al., 2002). To our knowledge, the formation of explosively developing twin
182 cyclones has been, to date, only observed and studied in the tropics (Ferreira et al., 1996;
183 Moustouli et al., 2002), in the mid-latitudes (Yokoyama and Yamamoto, 2019) and in the Arctic
184 (Renfrew et al., 1997). In this study, we report for the time, the formation of polar twin cyclones
185 near Antarctica during two consecutive events; one on 19-20 September 2019 at 60°E and the
186 second on 23-24 September 2019 at 85°E.

187 Despite the observed poleward shift of extratropical cyclones, the increasing number and intensity
188 of explosive cyclones around Antarctica and the decline in sea ice extent in recent years, the impact
189 of extreme cyclones on ice shelves instability has not been investigated to date.

190 Building on previous studies that investigated these patterns separately, we aim in this study to
191 assess the impact of extreme cyclone activity during the largest calving event since 1963 at the
192 Amery Ice Shelf. Using satellite data and atmospheric reanalyses, we investigate the role of
193 atmospheric forcings in this calving event which occurred under a ZW3-like situation. The
194 development of the explosive cyclones and their impact on sea ice and land ice conditions are
195 addressed in section 2. Section 3 discusses our findings. The data and methods used in this study
196 are described in section 4.

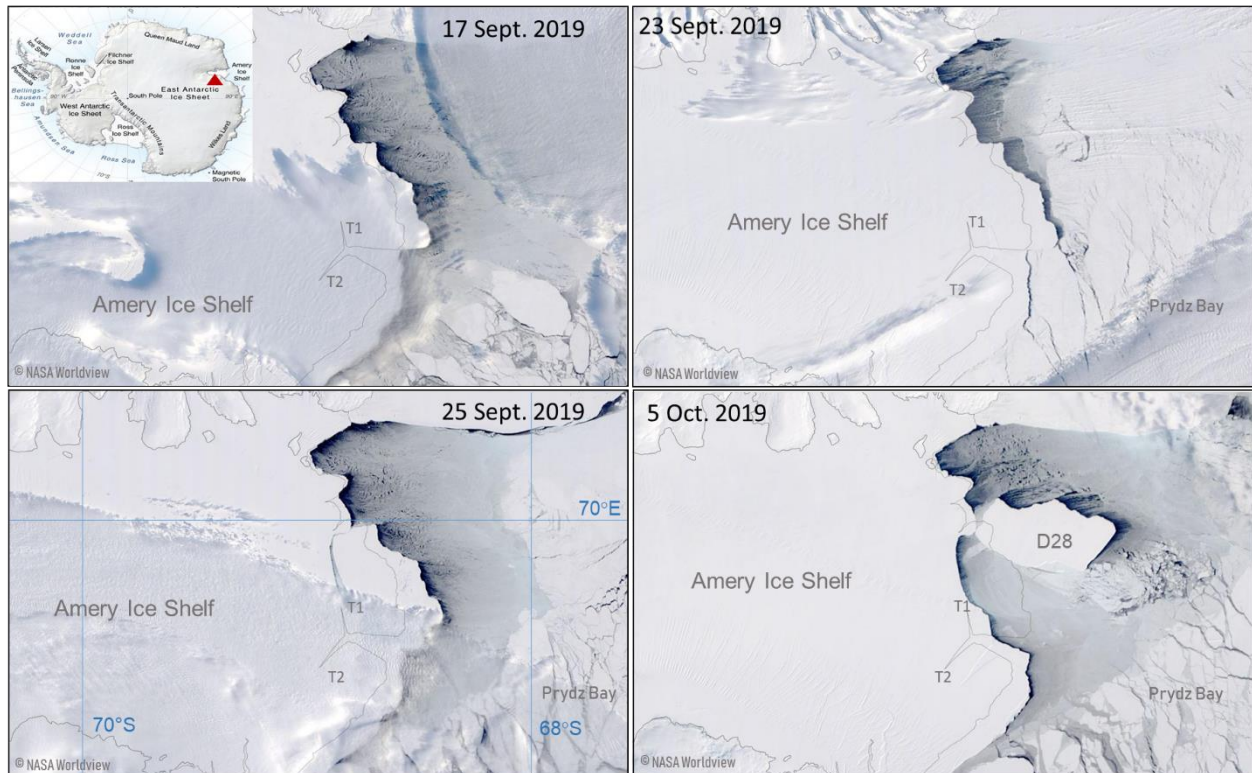


Figure 1: MODIS satellite visible imagery of the Amery Ice Shelf and the Loose Tooth rift system (T1 and T2) at its front. Ice conditions are shown before the calving on 17 and 23 September 2019, during the calving on 25 September 2019, and few days after the detachment of the new iceberg D28. Image credit NASA Worldview.

197

198 2. Results

199 2.1 Explosive twin cyclones during 18-22 September 2019 – preconditioning

200 In September 2019, the synoptic conditions exhibited an amplified zonal wave number 3 (ZW3)
 201 pattern characterized by 3 trough/ridge systems associated with low/high mean sea level pressure
 202 (MSLP) anomalies. Compared to all Septembers in the 1979-2019 period, the broad scale MSLP
 203 anomaly indicates that, for September 2019, there was below average pressure over much of the
 204 Antarctic continent and above average pressure to the north (Fig. 2a). In the Indian Ocean sector,
 205 the MSLP anomalies exceeded one standard deviation from the mean over large areas with the
 206 strongest troughing over Cooperation and Davis Seas (Fig. 2a). To the west of this low pressure
 207 anomaly, the South Atlantic ridge exhibited strong positive anomalies exceeding 2 standard
 208 deviations from the mean (Fig. 2a). To the east of the low pressure anomaly around the Amery Ice
 209 Shelf, another pronounced ridge encompassing south Australia and the Mawson Sea with positive
 210 MSLP anomalies exceeded 1 standard deviation from the climatological mean (Fig. 2a).

211 On a daily scale, the aforementioned synoptic setting was synonym of frequent and extreme
 212 weather systems. On 17 September 2019 at 0200 UTC, an extratropical cyclone associated with a
 213 968 hPa low-pressure at its center and located at 60°S, 40°E, started to deepen while moving
 214 poleward and eastward. It reached the western side of Cooperation Sea on 18 September 2019 at

215 0200 UTC with a 940 hPa minimum pressure and remained over this region the entire day (Fig.
 216 2b), then decayed on 19 September, with 980 hPa central pressure by 1300 UTC. The rapid
 217 deepening of the low pressure is characteristic of explosive cyclones (e.g., Sanders and Gyakum,
 218 1980). The explosive cyclone on 18 September 2019 was associated with significant poleward
 219 transport of moisture (Fig. 2c) and heat (Fig. 2d) carried by an atmospheric river propagating
 220 poleward adjacent to the low-pressure center. The atmospheric river was associated with integrated
 221 water vapor transport (IVT) greater than $500 \text{ kg m}^{-1} \text{ s}^{-1}$ at its core, with IVT values around 100 kg
 222 $\text{m}^{-1} \text{ s}^{-1}$ over Prydz Bay exceeding the 99th percentile of September climatology in this region (Fig.
 223 3a). The moisture and heat carried by the atmospheric river over the ice sheet may have caused
 224 warming at the surface due to condensation (released heat) as well as by increase in downward
 225 longwave radiation (e.g., Francis et al., 2020).

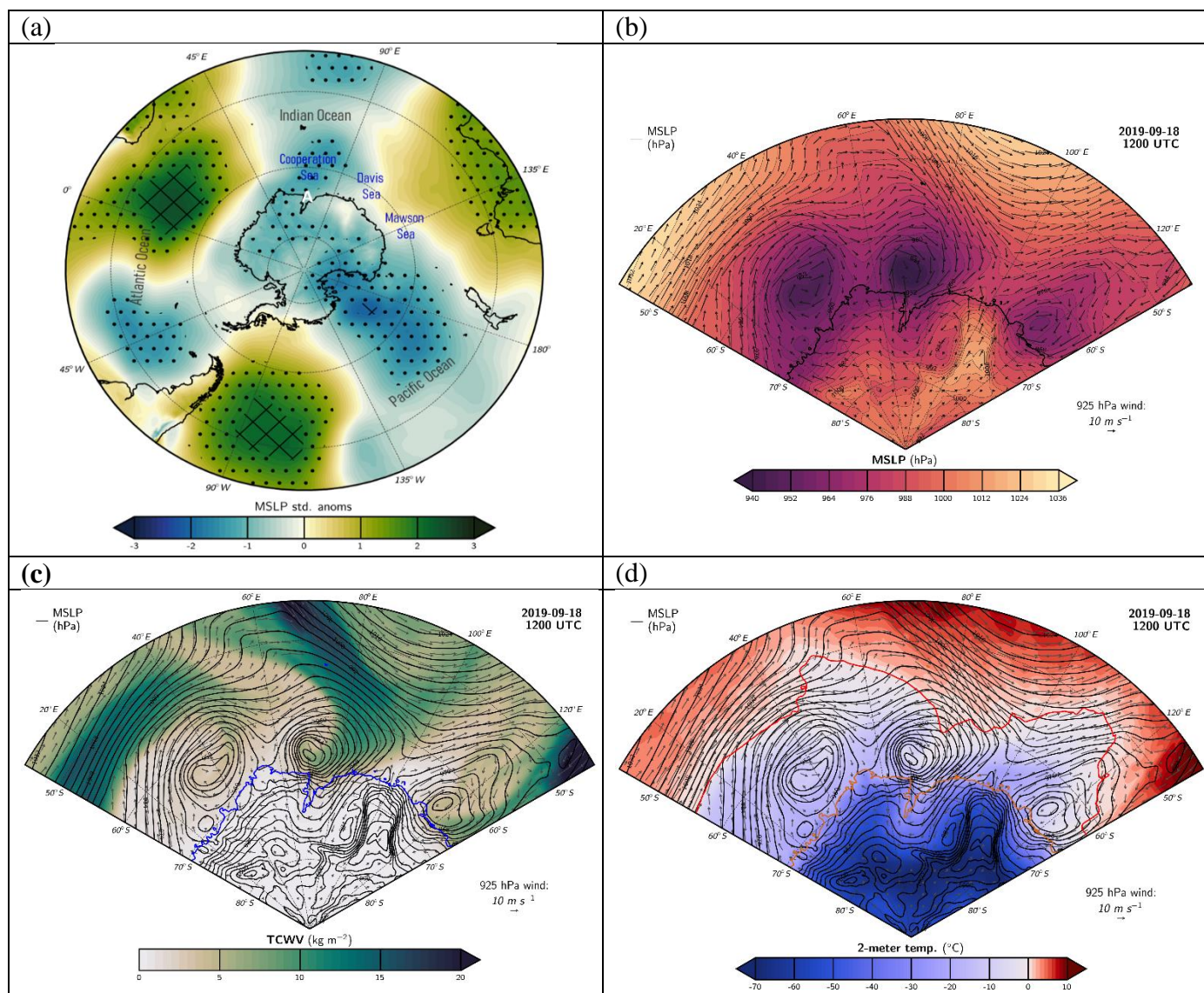


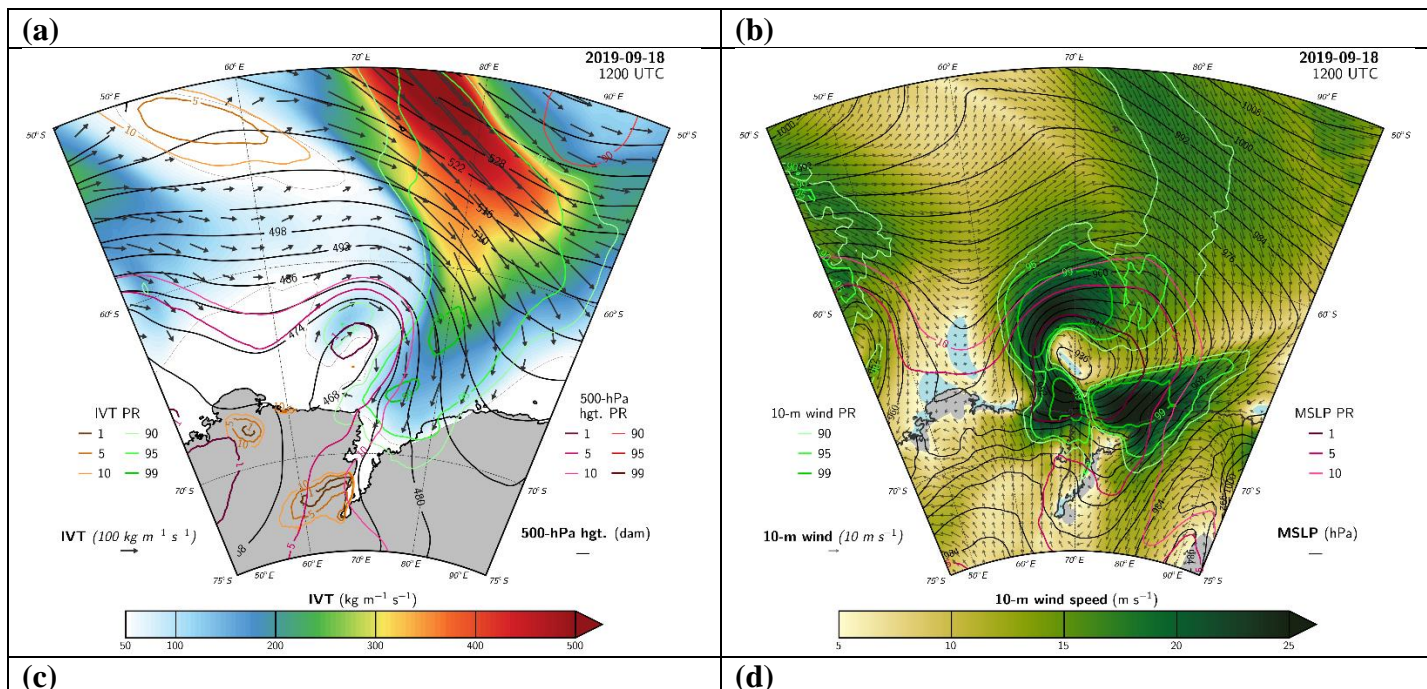
Figure 2: Normalized anomalies of Mean Sea Level Pressure (MSLP) for September 2019 relative to the 1979-2019 September climatology. Black dots are regions where the normalized anomalies are larger than 1 standard deviation from the mean and black squares are regions where the normalized anomalies are

larger than 2 standard deviations from the mean. The letter A in white indicates the location of the Amery Ice Shelf. (b) MSLP (shaded) and winds at 925hPa (vectors) at 18 September 2019 1200 UTC, (c) same as (b) but for the total column water vapor (TCWV) in colors, winds at 925hPa in vectors and MSLP in black contours, (d) same as (c) but for 2-m temperature (in colors), winds at 925hPa in vectors, MSLP in black contours and 0°C contour in red.

226

227 In the Southern Hemisphere, where cyclonic winds spin clockwise, the highest wind speed occurs
 228 along the bent-back front of the cyclone, i.e., to the left-west of the low-pressure center of the
 229 cyclone (e.g., Wagner et al., 2011, Watanabe and Niino, 2014). This was observed during the
 230 explosive cyclone on 18 September 2019 which generated extremely strong surface winds to the
 231 left-west of its center exceeding 20 m s^{-1} (Fig. 3b). Being stationary over Cooperation Sea but to
 232 the west of the Amery Basin, this extreme cyclone generated a sustained northeasterly wind stress
 233 over the northern part of the ice shelf (Fig. 3b), as well as strong poleward warm and moist air
 234 advection (Fig. 2c, 2d and 3a). The combination of warm temperatures brought by the cyclone/AR
 235 and strong easterly/northeasterly wind speeds was unusual (Fig. 3). MSLP anomalies during this
 236 event were in excess of -4 standard deviations (Fig. 3b), with MSLP values below the 1st percentile
 237 of September climatology over a large area along and to the north of the ice shelf margin (Fig. 3b).
 238 Extreme wind anomalies exceeding the 99th percentile over the central and eastern ice shelf margin
 239 were associated with this cyclone from 18 September through 19 September 2019 (Fig. 3c).
 240 Surface winds of 25 m s^{-1} , relative to 99 percentiles (5 standard deviations above the climatological
 241 mean), were registered during this event (Fig. 3b and 3c). Likewise, there were sustained positive
 242 2-m temperature anomalies throughout the period exceeding 2 standard deviations from the
 243 climatological mean (Fig. 3d).

244



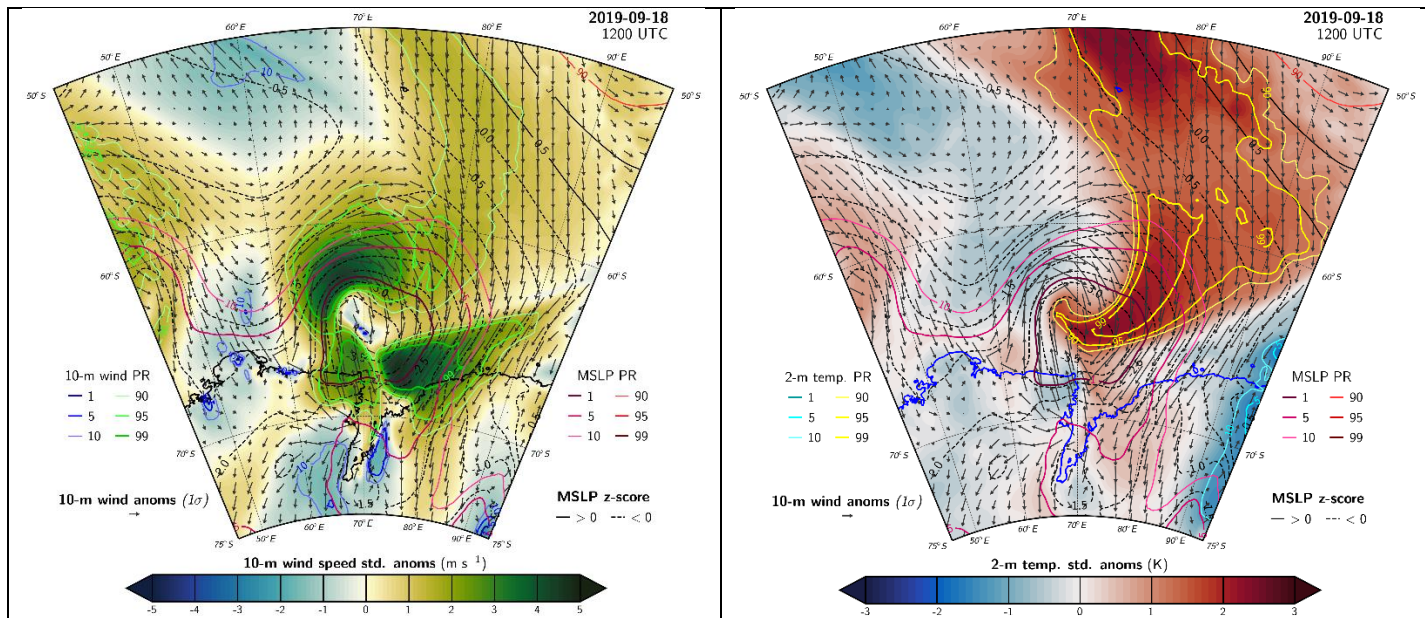


Figure 3: Maps on 18 September 2019 at 1200 UTC of (a) Integrated water vapor transport (IVT) shaded, geopotential heights at 500 hPa in black contours and IVT direction in black vectors, (b) 10-m wind speed in colors, 10-m wind direction in black vectors and MSLP in black contours. (c) Standardized 10-m wind speed anomalies relative to the full September record (1979-2019) (d) Same as (c) but for 2-m temperature. Colored contour lines show percentile rank extremes (1, 5, 10 and 90, 95, 99 percentile ranks) of the corresponding quantities indicated on the plots. On (c) and (d): Vectors show 10-m wind anomalies, black contours show positive MSLP anomalies and dashed black contours show negative MSLP anomalies.

245

246 The first explosive cyclone on 18 September 2019 was followed immediately by a second
 247 explosive cyclone which approached Cooperation Sea from the west on 19 September at 1400
 248 UTC with a deep low of 952hPa. At 2000UTC, this deep cyclone widened and evolved into two
 249 twin polar cyclones over the same region (Fig. 4a). The twin cyclones exhibited 960hPa low-
 250 pressure at their respective centers and remained active to the west of the Amery Ice Shelf for three
 251 consecutive days (Fig. 4a). Their signatures dissipated in the pressure field on 22 September 2019
 252 at 0000UTC. The poleward transport of heat (Fig. 4b) and moisture (Fig. 4c) towards the Amery
 253 Ice Shelf continued during this event together with extreme wind stress exceeding the 99th
 254 percentile (Fig. 4d). Being stationary to the west of the Amery Ice Shelf (Fig. 4a), the twin cyclones
 255 induced extreme easterly winds across the ice shelf, with u-wind anomalies exceeding -5 standard
 256 deviations of September climatology over the western ice shelf from 19 September 2019 at 1900
 257 UTC through 20 September at 1100 UTC (Fig. 4d) and below the 1 percentile u-wind values over
 258 the whole lower ice shelf area (Fig. 4d). When compared with the climatology for all months
 259 during 1979-2019, many hourly wind speeds over the ice shelf front during 18-20 September were
 260 substantially greater than the 99th percentile of climatology, with the most anomalous wind speeds
 261 on 18 September (Fig. 6e).

262 On 21 September 2019, the twin cyclones merged and moved to the area in front of the Amery Ice
 263 Shelf (Fig. 4e) resulting in a deep cyclone associated with MSLP at its center below the 5th
 264 percentile. The remnant cyclone slowly meandered along the northern margin of Prydz Bay

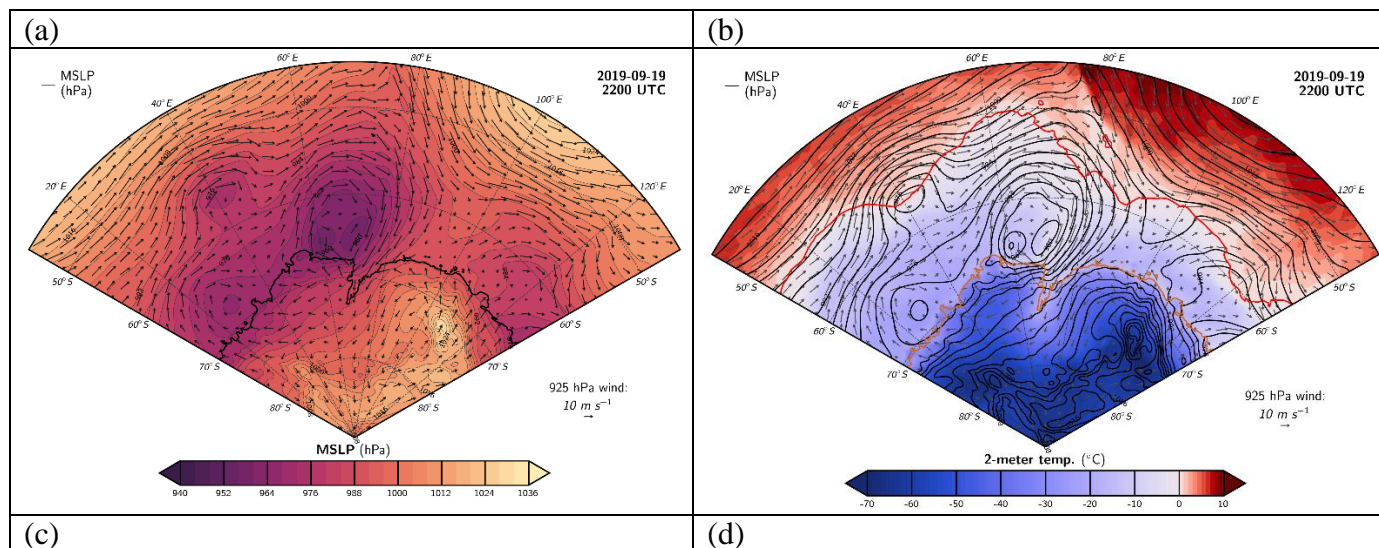
265 and decayed on 22 September 2019. Anomalously warm air masses were brought by this cyclone
 266 over the margins of the Amery Ice Shelf exceeding the 90th percentile (Fig. 4e). MODIS satellite
 267 imagery on this day showed a swirling cyclone at the mouth of the Amery Ice Shelf (Fig. 4f).
 268 Sentinel-3A and 3B observations on 22 September 2019 at 0000 UTC (i.e., during the decay of
 269 the cyclones) show elevated sea surface at the ice-shelf front area reaching 6 m significant wave
 270 height (Fig. 4g). Given the easterly direction of the winds associated with the storm during this
 271 episode, the observed elevation of sea surface indicates that storm tide occurred at the ice shelf
 272 front. Furthermore, waves and tides generated by the cyclones during the 18-21 September 2019
 273 period, when easterly wind speeds were stronger, may have been substantially higher.
 274 Unfortunately, sentinel observations are not available during this period over the area of interest
 275 to check this.

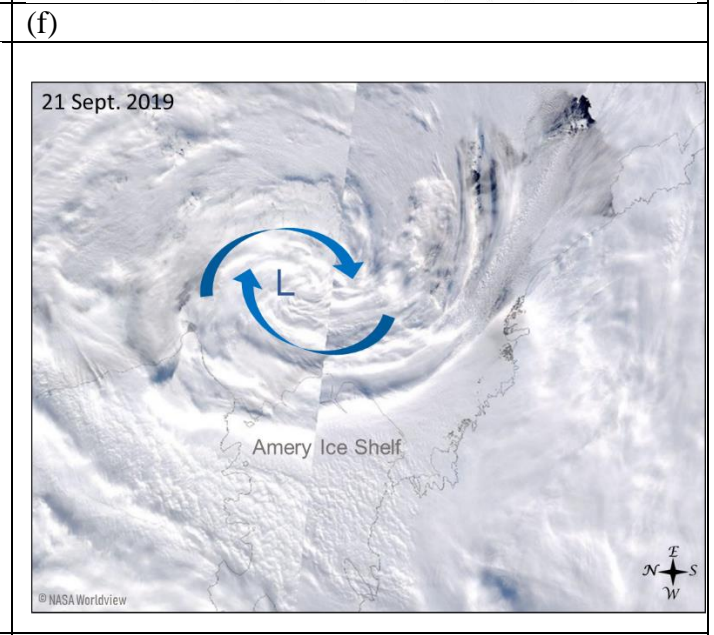
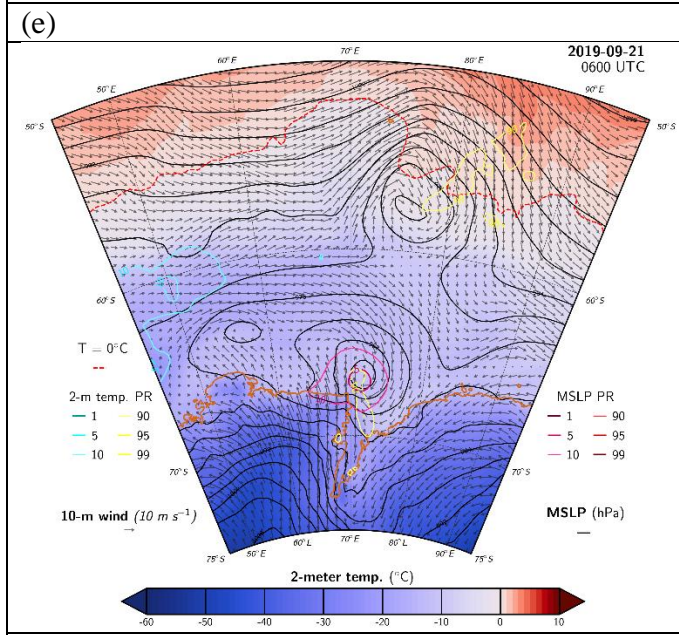
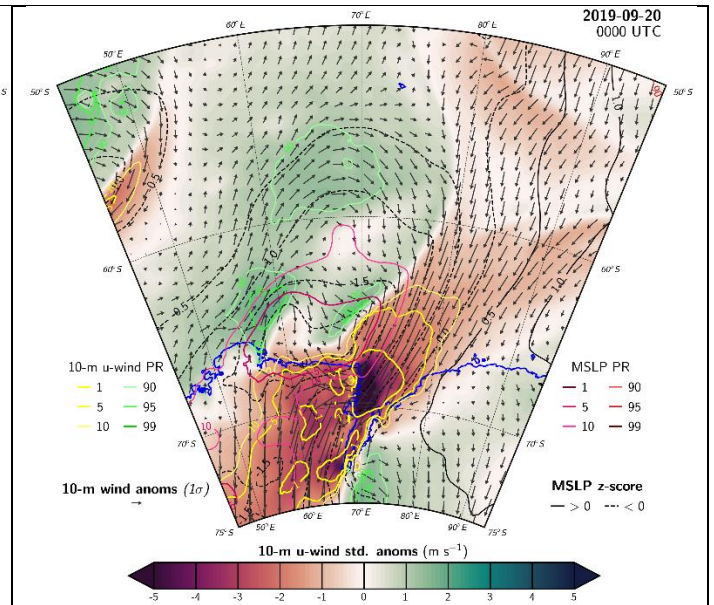
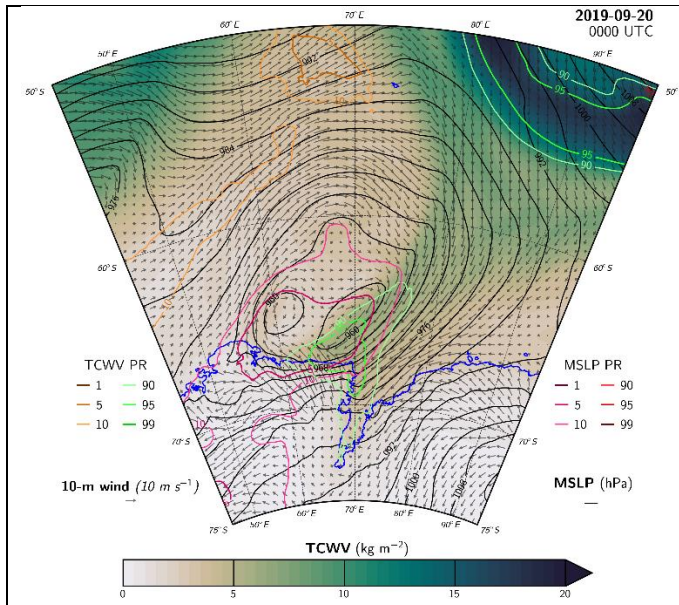
276 Surface melt during this event may have occurred briefly due to the anomalous warm and moist
 277 air masses. However, the inspection of daily satellite images of Sentinel-1 backscatter coefficient,
 278 MODIS ice surface temperature and AMSR2 brightness temperature did not show any prolonged
 279 nor significant surface melt at the Amery Ice Shelf during this event.

280 In summary, an extended period of strong cyclonic activity from 18-22 September 2019 resulted
 281 in exceptional period of strong easterly / northeasterly winds over the western side of the Amery
 282 Ice Shelf where the climatology shows a positive zonal component. Theise exceptional winds
 283 stress on the ice shelf generated significant storm surge onto the ice shelf and helped in
 284 preconditioning the breakoff as it will be discussed in section 2.3.

285 strong waves in the region in front of the ice shelf. The advection of anomalous warm and moist
 286 air masses to the area at the ice shelf front may have contributed to a decrease in sea ice
 287 concentration at the front of the ice shelf, as it will be shown in section 5.

288





(g)

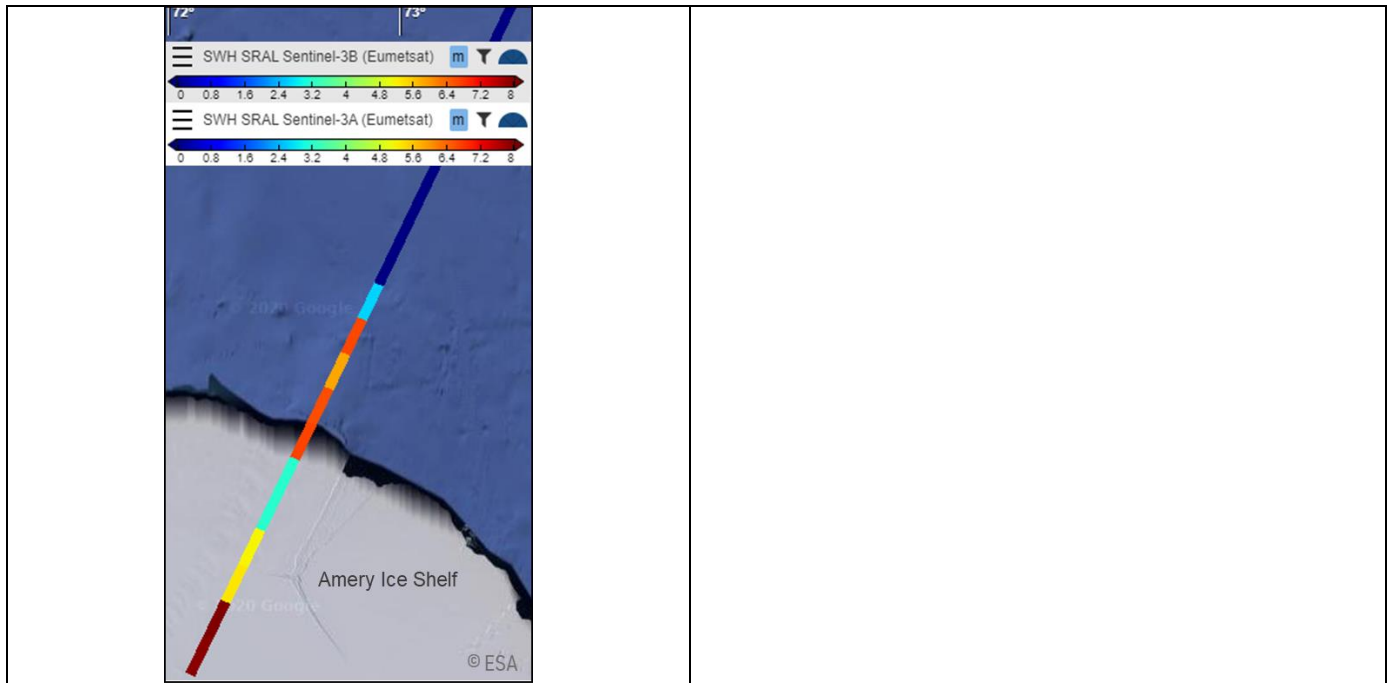


Figure 4: ERA5 reanalysis of: (a) MSLP in colors and winds at 925hPa in vectors on 19 September 2019 at 2200 UTC, (b) 2-m temperature in colors, winds at 925hPa in vectors, MSLP in black contours and 0°C contour in red on 19 September at 2200 UTC, (c) total column water vapor (TCWV) in colors, winds at 925hPa in vectors and MSLP in black contours on 20 September 2019 at 0000 UTC, (d) standardized anomalies relative to the full record (1979-2019) of 10-m u-wind on 20 September 2019 at 0000 UTC. Vectors show 10-m wind anomalies, black contours show positive MSLP anomalies and dashed black contours show negative MSLP anomalies. Colored contour lines show percentile rank extremes (1, 5, 10 and 90, 95, 99 percentile ranks) of the corresponding quantities indicated on the plots, (e) 2-m temperature in colors, 10-m winds in vectors, MSLP in black contours and 0°C contour in red dashed-line on 21 September at 0600 UTC. (f) MODIS visible imagery on 21 September 2019, image credit: NASA worldview. (g) Sentinel-3A and 3B observations of wave height on 22 September 2019 at 0000 UTC, image credit: ESA Ocean Virtual Laboratory.

289

290 **2.2. Twin polar cyclones during 23-24 September 2019 - calving**

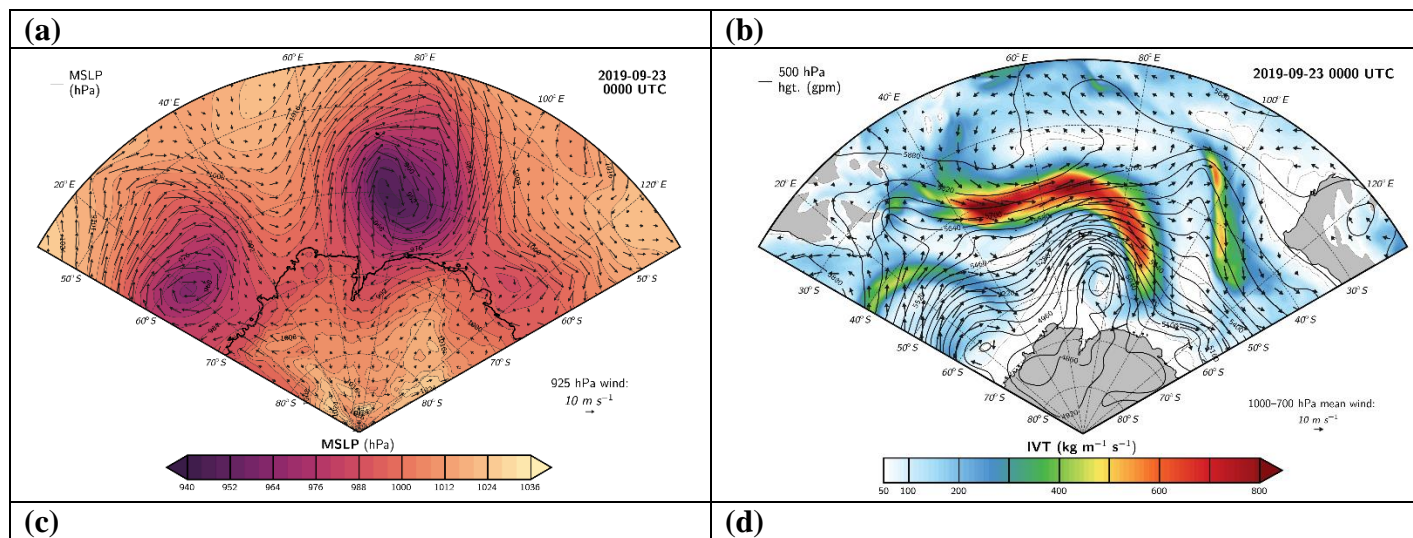
291 Following the extended period of extreme cyclones in Cooperation sea, an explosive cyclone
 292 started to develop on 21 September 2019 centered at 45°E and 60°S. The pressure at its center
 293 deepened from 976hPa on 21 September at 1900 UTC to 952hPa on 22 September 2019 at 19 UTC
 294 (not shown). On 23 September 2019, the large explosive cyclone entered Cooperation Sea from
 295 the west with a deep low of 940 hPa (Fig. 5a). It was accompanied by an intense atmospheric river
 296 exhibiting core IVT greater than $800 \text{ kg m}^{-1} \text{ s}^{-1}$ and stretching from mid-latitudes towards
 297 Antarctica (Fig. 5b). The explosive cyclone was stationary over Cooperation Sea during the whole
 298 day on 23 September 2019, being trapped between two far-south-reaching blocking ridges-highs
 299 one to the west of it and the second to its east (Fig. 5a and 5c). The cyclone intensified, increased
 300 in size and evolved into twin cyclones on 24 September 2019 at 0000 UTC associated with 952hPa
 301 low pressure at their respective centers (Fig. 5c and 5d). The mutual interaction between the two
 302 cyclones appeared as co-rotation and an eastward translation of the binary pair by the ambient

303 flow. The interplay between the cyclones lasted for one day after which the twins merged and
304 decayed on 25 September 2019.

305 To the south of the twin cyclones, a cold pressure high (1036 hPa) developed over the ice sheet as
306 a result of the accumulation of cold air due the blocking ridge to the northeast (Fig. 5c). The high-
307 pressure advected ~~extremely-very~~ cold air masses (2-m temperature below -40°C) into the twin-
308 cyclone system (Fig. 5e and 5 f) which may have fostered baroclinicity and frontogenesis, hence
309 sustaining the twin cyclones for a longer period of time.

310 The atmospheric river continued to advect large amounts of moisture and precipitation occurred
311 over a large area (Fig. 5d). ~~Transport of moisture from mid latitudes toward East Antarctica~~
312 ~~continued during this period and high precipitable water amounts were continuously advected by~~
313 ~~the atmospheric river and the cyclones over the ice shelf margins~~ Sustained advection of
314 exceptionally warm air masses was observed during this event as well (Fig. 5e and 5f). Air masses
315 characterized by 0°C 2-m temperatures were seen to penetrate further south reaching 66°S over
316 the region to the east of the twin cyclones during the whole day on 24 September 2019 (Fig. 5e
317 and 5f).

318



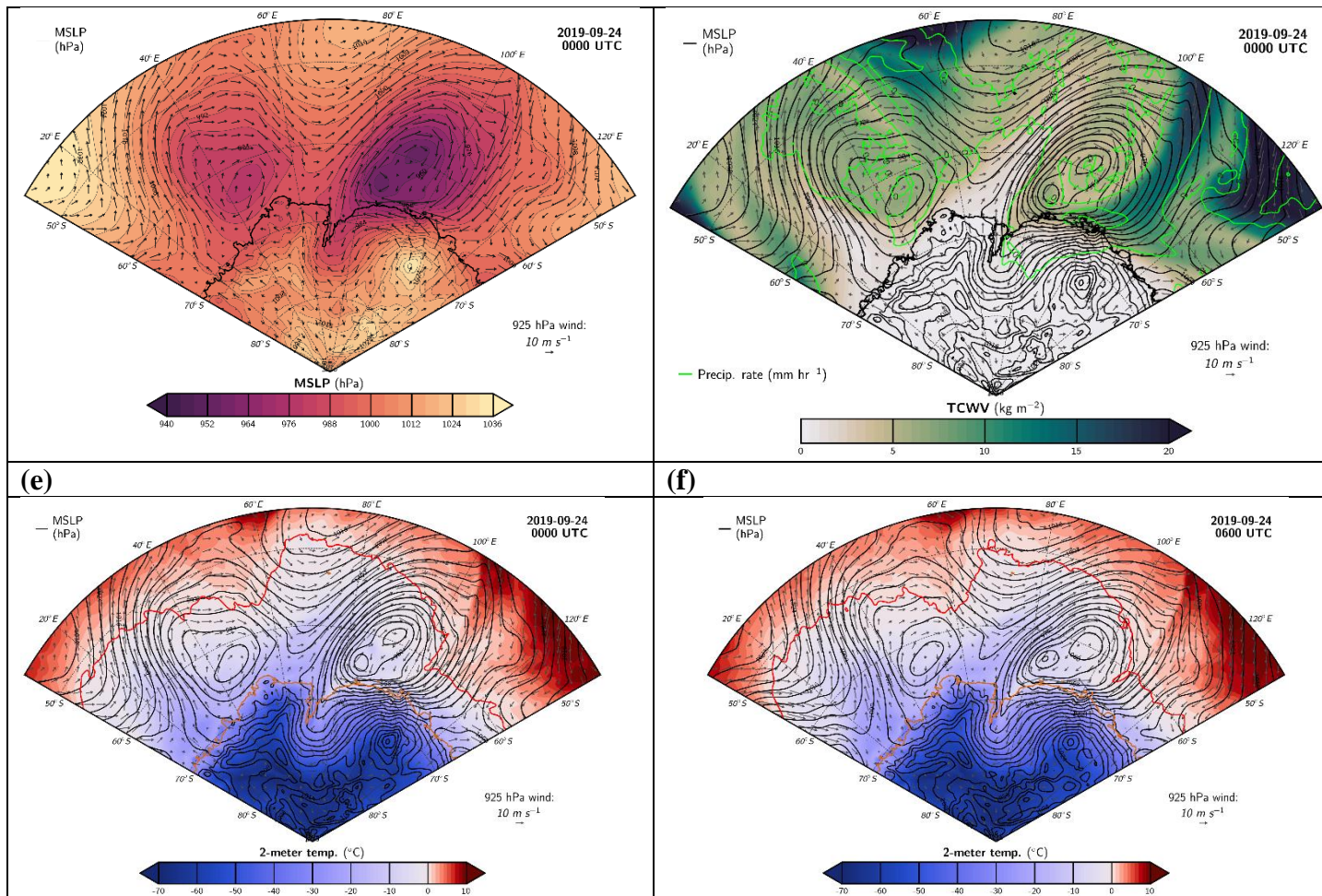


Figure 5: (a) MSLP in colors and winds at 925hPa in vectors on 23 September 2019 at 0000 UTC, (b) integrated water vapor transport (IVT) in colors, geopotential heights at 500 hPa in black contours and 1000-700 hPa mean winds in black vectors on 23 September 2019 at 0000 UTC, (c) MSLP in colors and winds at 925hPa in vectors on 24 September 2019 at 0000 UTC, (d) total column water vapor (TCWV) in colors, winds at 925hPa in vectors, precipitation rate in green contours and MSLP in black contours on 24 September 2019 at 0000 UTC, (e) 2-m temperature in colors, winds at 925hPa in vectors, MSLP in black contours and 0°C contour in red on 24 September at 0000 UTC, (f) same as (e) but at 0600 UTC.

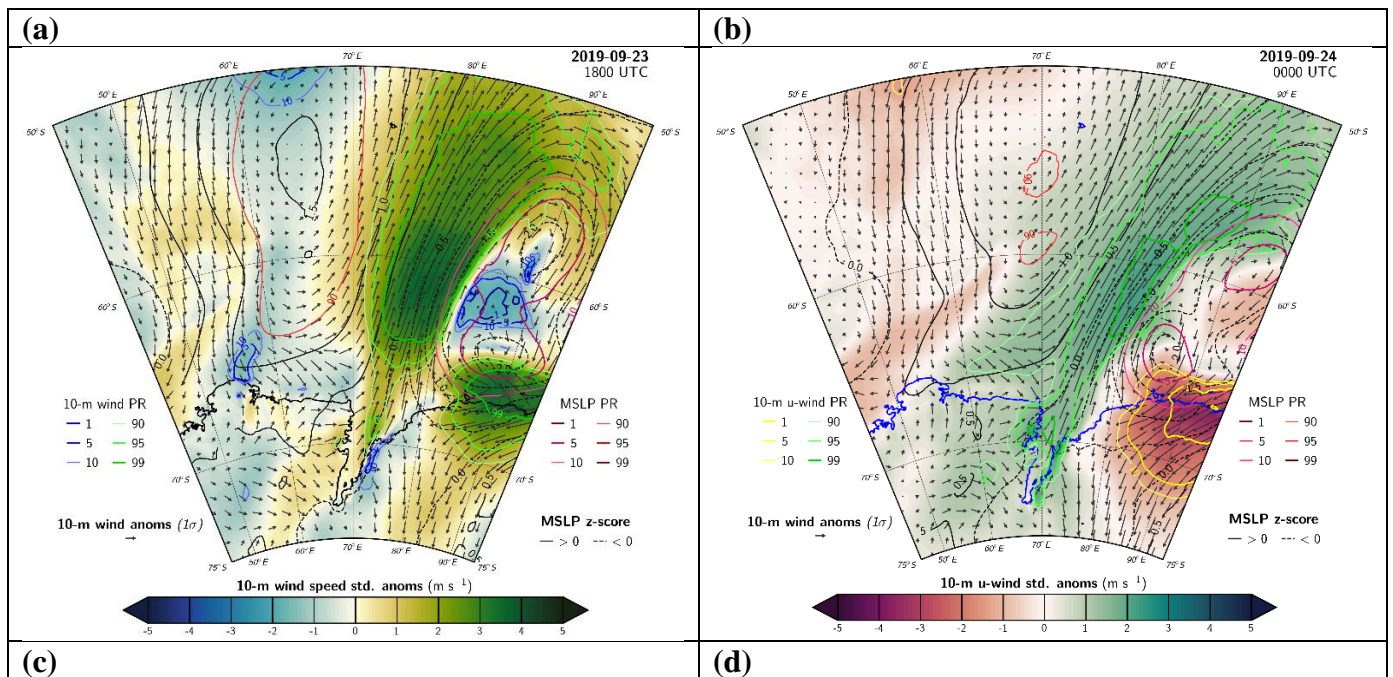
319

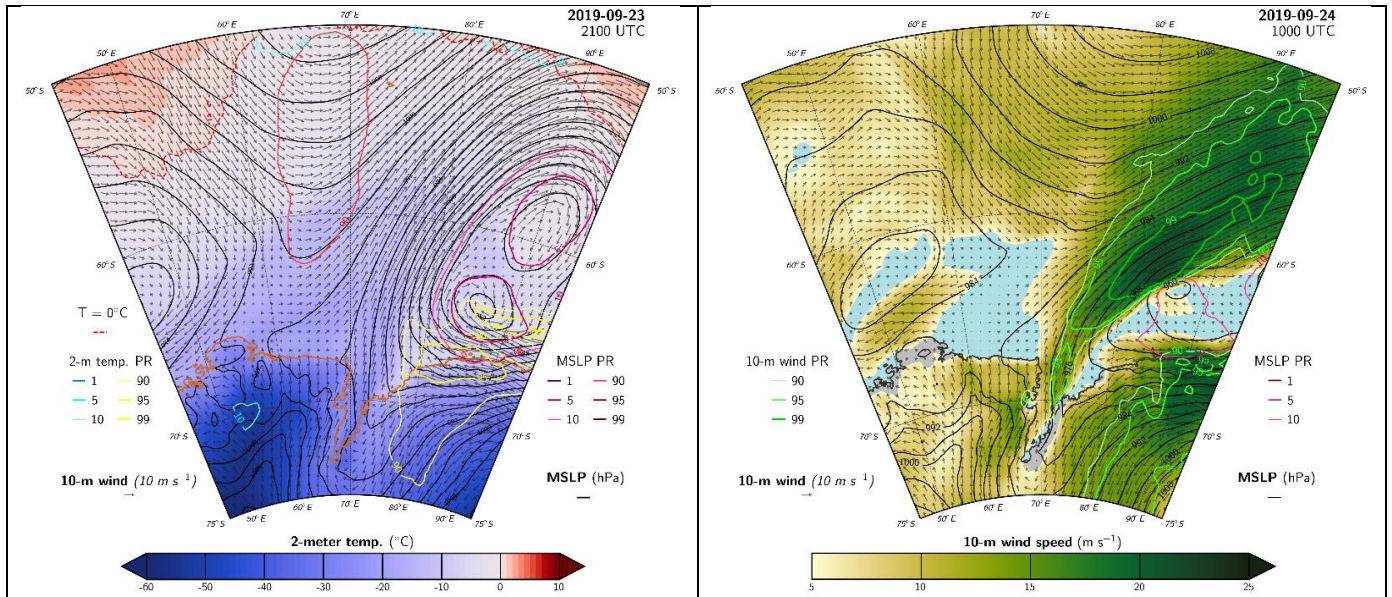
320 During 23-24 September, the deep twin polar cyclones were stationary to the east of the Amery
 321 Ice Shelf (Fig. 5) associated with MSLP anomalies at their centers below the 5th percentile (Fig.
 322 6a and 6c). They induced extreme westerlies (10-m wind speed in the order of 17 m s^{-1}) across the
 323 ice shelf with positive 10-m wind anomalies exceeding 2 standard deviations from the
 324 climatological mean (Fig. 6a). The direction of the winds was also exceptional with above 99th
 325 percentile u-wind over the western ice shelf margin from 23 September 2019 at 1800 UTC (Fig.
 326 6b) through 24 September 2019 at 1200 UTC and below the 5th percentile u-wind values over the
 327 lower eastern ice shelf area (Fig. 6a and 6b). Weaker but still significant (95 percentile) westerly
 328 wind anomalies lingered during the remainder of the day on 24 September 2019 and through
 329 midday on 25 September 2019 with wind speed at 10-m reaching 15 m s^{-1} at the front of the ice
 330 shelf (Fig. 6d). Sustained positive 2-m temperature anomalies were observed throughout the twin

331 cyclone event over the eastern side of Prydz Bay. Warm air advection by the twin cyclones brought
 332 95 percentile rank temperatures over the eastern side of the Amery Ice Shelf and Prydz Bay on 23
 333 and 24 September 2019 and 90 percentile rank temperatures inland over Princess Elizabeth Land
 334 (Fig. 6c). These episodes of poleward advection of warm air masses may explain the observed
 335 positive-trend in surface temperatures during winter/spring seasons at Prydz Bay reported by Heil
 336 (2006) using measurements from ground stations.

337 The distribution of hourly 10-m wind speed for all months 1979-2019 over the Amery Ice Shelf
 338 front is shown in the histogram in Fig. 6f. The winds during the 18-22 September 2019 period
 339 were exceptionally unusual compared to the record. The winds during the 23-25 September 2019
 340 period were strong but not unusually extreme. This suggests that the first extreme cyclones' event
 341 had an important role in preconditioning the ice shelf front for breakoff, while the offshore winds
 342 during the second event triggered the calving along the T1 rift.

343





(e)

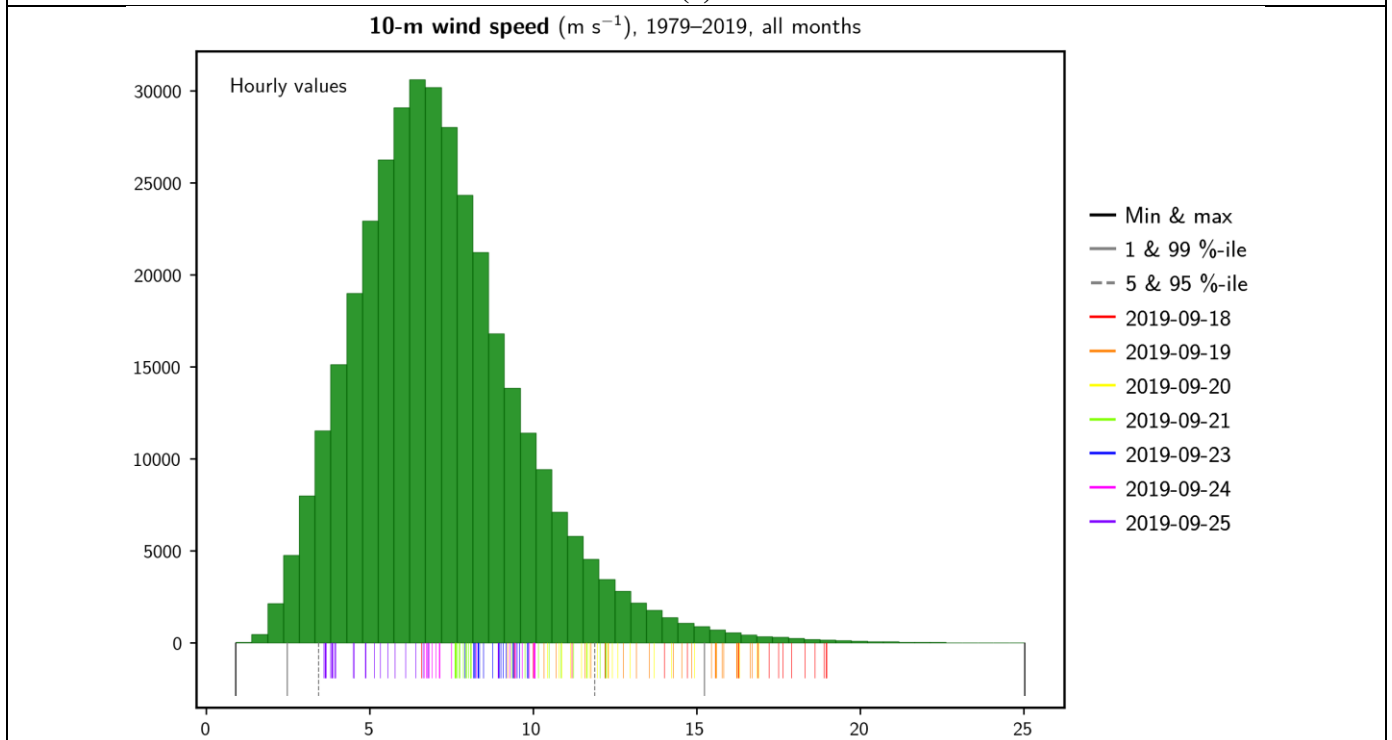


Figure 6: (a) Standardized anomalies relative to the full September record (1979-2019) of 10-m wind speed (colors) at 23 September 2019 1800 UTC. (b) Same as (a) but with u-component of 10-m wind as filled contours at 24 September 2019 0000 UTC. Vectors show 10-m wind anomalies, black contours show positive MSLP anomalies and dashed black contours show negative MSLP anomalies. Colored contour lines show percentile rank extremes (1, 5, 10 and 90, 95, 99 percentile ranks) of the corresponding quantities indicated on the plots. (c) 2-m temperature in colors, winds at 925hPa in vectors, MSLP in black contours and 0°C contour in red dashed-line on 23 September at 2100 UTC. (d) 10-m wind speed in colors, 10-m wind direction in black vectors and MSLP in black contours on 24 September 2019 at 1000 UTC. (e) Histogram showing the distribution of hourly 10-m wind speed for all months during 1979-2019,

spatially averaged over 70-65°S and 70-75°E. The colored vertical lines correspond to hourly values during the 18-25 September 2019 period. Each given day in September 2019 has 24 hourly values plotted in the same color.

344

345 **2.3 The calving**

346 The anomalous atmospheric conditions during the extended period of strong cyclonic activity
347 occurring over the ice cover in Cooperation and Davis Seas (i.e., south to the sea ice edge)
348 impacted the state of the ocean in front of and around the Amery Ice Shelf. The storm surge caused
349 by the first twin cyclones (i.e., Fig. 4g) was followed by an ocean ward slope induced by the second
350 episode of cyclones. Fig. 7a shows a clear increase in maximum ocean slope close to the Amery
351 Ice Shelf in the period prior to the calving. The wind pattern of 23-24 September induced a
352 significant slope on the ocean surface at/near the ice front. This ocean ward slope tugs on the ice
353 front, placing extensional stress on the pre-existing rift. The SAR satellite image on 23 September
354 2019 together with the ice-displacement velocity (rate and direction in vectors) relative to 11
355 September 2019 are shown in Fig. 7b. The displacement vectors indicate that the iceberg-to-be
356 was rotating in the period 11-23 September 2019 prior to the calving. Wind-induced ocean slope
357 caused a leftward (relative to the rift T1) splitting-movement of the future iceberg prior to break-
358 off on 25 September 2019. This caused rapid opening of the crack and subsequent movement of
359 the iceberg away from the ice shelf (Fig. 8a).

360 The extreme nature and long duration of the cyclones during both cyclones' episodes resulted in
361 sustained tides and ocean ward slope of the sea surface, consecutively. Between the previous storm
362 event and the 23-24 September storm, there was a rapid change from a shoreward surge to ocean
363 slope away from the ice front. This put strain on the pre-existing rift at the front of the Amery Ice
364 Shelf leading to rift growth and calving.

365 ~~had significant impacts on both sea ice and land ice (Fig. 7). The sustained period of strong~~
366 ~~cyclonic activity occurring over the sea ice pack and onto the Amery Ice Shelf caused decreases~~
367 ~~in sea ice concentration both at the mouth of the Amery Ice Shelf and further offshore. Although~~
368 ~~this study focuses on the period 17-25 September 2019, the inspection of the sequence of MODIS~~
369 ~~images for the whole month of September 2019 revealed several episodes of sea ice removal from~~
370 ~~the ice shelf front area during the 7-17 September 2019 period by offshore winds (i.e., Fig. 1).~~
371 ~~Despite the formation of new sea ice over the area, the sea ice removal may have preconditioned~~
372 ~~the sea ice cover for further reduction during the subsequent series of extremes cyclones and~~
373 ~~increased the area of open water susceptible to ocean wave activity along the front of the ice shelf.~~

374 ~~Sea ice concentration in Cooperation Sea and at the Amery Ice Shelf front area was reduced to~~
375 ~~below 60%, reaching 40% in some places (Fig. 7a and 7b). By the end of the intense cyclonic~~
376 ~~activity period, areas of open water formed especially at the locations of the strongest surface~~
377 ~~winds i.e., to the left of the twin cyclones centers (Fig. 7c and 7d). Significant reduction in sea ice~~
378 ~~concentration was also observed along the sea ice edge associated with wind driven currents and~~
379 ~~waves (Fig. 7) which may have decreased the sea ice attenuation effect of waves in ice~~
380 ~~propagating from lower latitude ocean toward the ice shelf.~~

381 The decrease in sea ice concentration was due to both sea ice melt caused by the anomalous warm
382 and moist air masses advected over the Amery Ice Shelf during the first episode of twin cyclones
383 (i.e., Fig. 3 and 4) and to sea ice drift out of the region by strong winds during the second episode
384 of twin polar cyclones (i.e., Fig. 5 and 6). The strong waves generated locally in the area of reduced
385 sea ice concentration in front of the ice shelf during the first set of cyclone events (Fig. 4h), were
386 important in preconditioning the breakoff by inducing flexure at the front.

387 Significant sea ice drift was observed at the mouth of the Amery Ice Shelf associated with the
388 exceptional westerlies generated by the twin cyclones on 23–24 September 2019 (Fig. 7e and 7d).
389 The sea ice drift velocity during this period reached 50 km on average per day and the sea ice
390 drifted away from the Amery Ice Shelf towards the east and northeast (Fig. 7f).

391

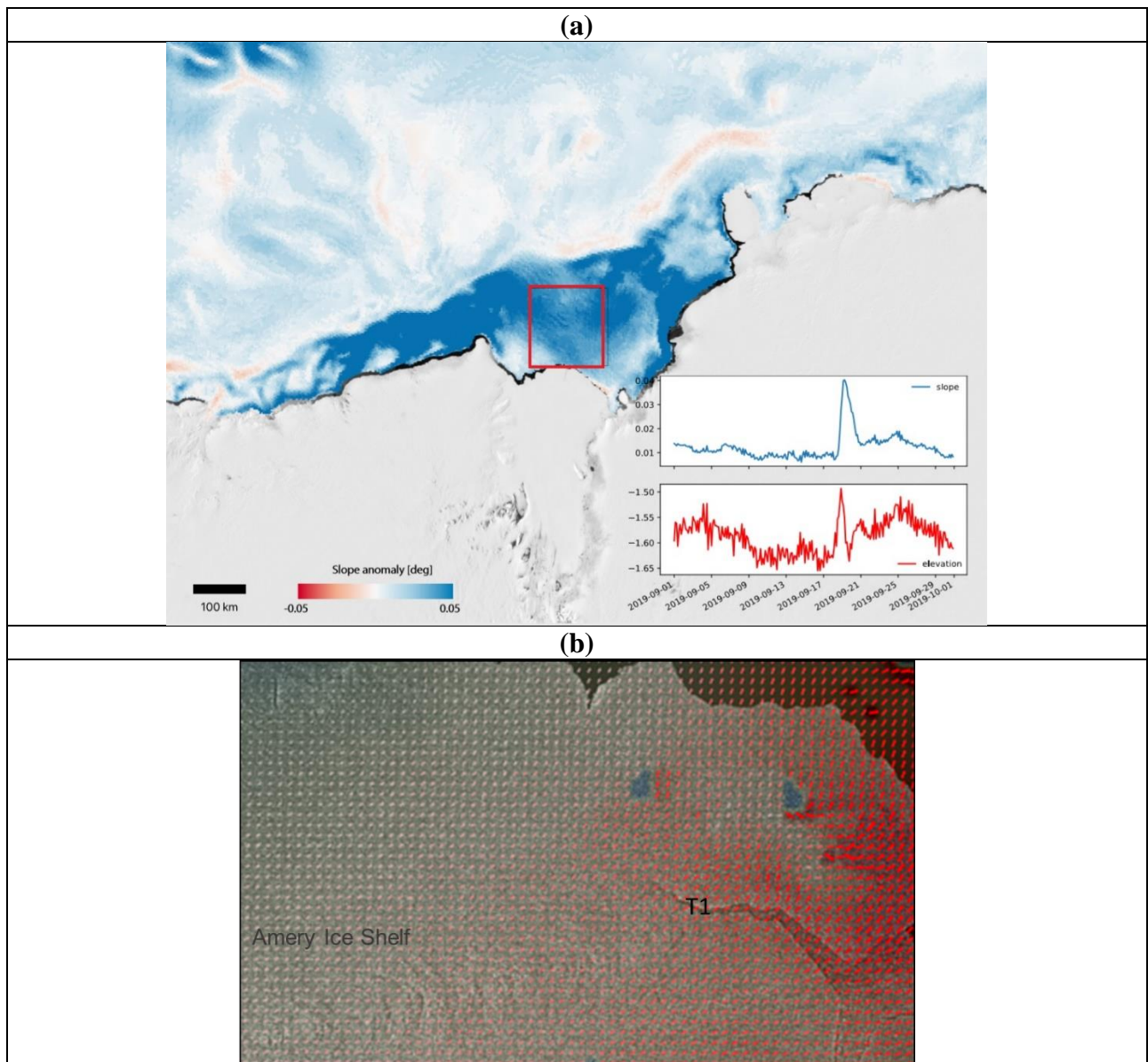


Figure 7: (a) 2D map of maximum ocean slope anomaly derived from HYCOM reanalysis dataset during the period 17-20 Sep 2019 relative to Sep 2019 mean and time series of slope and surface elevation over the red bounding box showed on the map. (b) SAR image of the Amery Ice Shelf on 23 September 2019. The red vectors correspond to the ice displacement on 23 September 2019 (both velocity and direction) relative to 11 September 2019.

392

393 2.4 Sea ice conditions

394 The action of strong winds on sea ice removal from the area at the mouth of the Amery Ice Shelf
395 was visible in MODIS imagery as well as in the satellite observations of sea ice concentration and
396 drift (Fig. 8). During the period of the twin polar cyclones on 23- 24 September 2019, the sea ice
397 was pushed about 65 km away from the ice shelf front in just a 2-day period of time (Fig. 8a). The
398 ice-free region in front of the ice shelf presented an asymmetric shape where the sea ice in front of
399 the western side of the ice shelf was pushed further away compared to the sea ice in front of the
400 eastern side (Fig. 8a). This may have made the western side more vulnerable to the winds and
401 associated tide/ocean slope induced by the consecutive explosive cyclones.

402 Moreover, sea ice concentration in Cooperation Sea and at the Amery Ice Shelf front area was
403 reduced to below 60%, reaching 40% in some places (Fig. 8b and 8c). By the end of the intense
404 cyclonic activity period, areas of open water formed especially at the locations of the strongest
405 surface winds i.e., to the west of the twin cyclones centers (Fig. 8b and 8c). Significant reduction
406 in sea ice concentration was also observed along the sea ice edge associated with wind-driven
407 currents and waves (Fig. 8b) ~~which may have decreased the sea ice attenuation effect of waves~~
408 ~~in ice propagating from lower latitude ocean toward the ice shelf.~~

409 Significant sea ice drift was observed at the mouth of the Amery Ice Shelf associated with the
410 exceptional westerlies generated by the twin cyclones on 23-24 September 2019 (Fig. ~~8c7e and~~
411 ~~7d~~). The sea ice drift velocity during this period reached 50 km on average per day and the sea ice
412 drifted away from the Amery Ice Shelf towards the east and northeast (Fig. ~~7f8c~~).

413 ~~In fact, s~~Sea ice loss in the vicinity of weakened or flooded shelves is considered as a contributor
414 factor to the ultimate cause of rapid ice shelf calving (e.g., Massom et al., 2018). The removal of
415 the protective buffer represented by sea ice for ice shelves (e.g., Massom et al., 2018) may have
416 increased the effect of the ocean ward slope on ~~enabled increased flexure of the~~ the outer ice shelf
417 western margin by wind induced waves and helped in the gravitationally-induced calving.

418 Explosive cyclones crossing the sea ice zone around Antarctica can generate waves of up to 8
419 meters in height that are capable of propagating more than 100 km into the sea ice cover (Vichi et
420 al., 2019). The consecutive deep cyclones under scrutiny impacted immediately the Amery Ice
421 Shelf front since they were found very close to the coast. During the first period of explosive twin
422 cyclones, the cyclones were sitting to the west of the Amery Ice Shelf which directed anomalous
423 warm and moist easterlies towards it. This situation caused shoreward storm surge and tide
424 immediately at the shelf front (Fig. 4g). This was then followed by additional extreme atmospheric
425 forcing brought by the second event of explosive twin cyclones, producing strong offshore winds,

426 sea ice removal and oceanward sea surface slope. This combination of factors weakened the ice
427 shelf front and made it more vulnerable, resulting in amplification of the fractures along the pre-
428 existing rifts and leading ultimately to its calving.

429 Previous studies (Holdsworth and Glynn, 1978; Squire et al., 1994) have shown that calving ice
430 shelves can be triggered by wind-induced waves which impose flexural strains on the ice shelves,
431 with the potential to induce crevasse and rift propagation and calving (Robinson and Haskell, 1992;
432 Bromirski et al., 2010). This effect can be even maximized by the loss of the protective sea ice
433 pack at the front of the ice shelves (Massom et al., 2018). Here we have shown that the series of
434 intense cyclones provided ideal conditions for both sea ice reduction, wind-tides and ocean slope
435 and ultimately triggered the calving on 25 September 2019.

436 ~~Furthermore, ocean swell (defined as relatively long period surface gravity waves that are
437 generated by distant weather systems and are no longer growing or being sustained locally by the
438 wind, as opposed to locally generated wind waves), may have also contributed to (i) fragilizing
439 the western side of the Amery Ice Shelf on 22 September 2019 (i.e., after the decay of the first two
440 twin cyclones) and to (ii) the calving on 25–26 September (i.e., after the decay of the second pair
441 of deep cyclones). Moreover, swells are strongly attenuated by the presence of extensive sea ice
442 which reduced substantially their destructive effect. Thus, loss of sea ice can maximize swell effect
443 on ice shelves. This mechanism has been found at work during the calving events of other Antarctic
444 ice shelves. A study on the calving event in March 1990 at the Erebus Glacier Tongue in the Ross
445 Sea implicated the removal of sea ice combined with ocean swell (Robinson and Haskell, 1990).
446 Focusing on the disintegration of the Larsen ice shelves, Massom et al., (2018) found that regional
447 loss of sea ice before and during the disintegration events allows storm-induced long period (10–
448 20 s) ocean swells to reach exposed ice shelf fronts that have been preconditioned for calving by
449 extensive fracturing and meltwater flooding. These swells excite flexural oscillations in the outer
450 ice shelf margin which amplify fracture and trigger a calving.~~

451

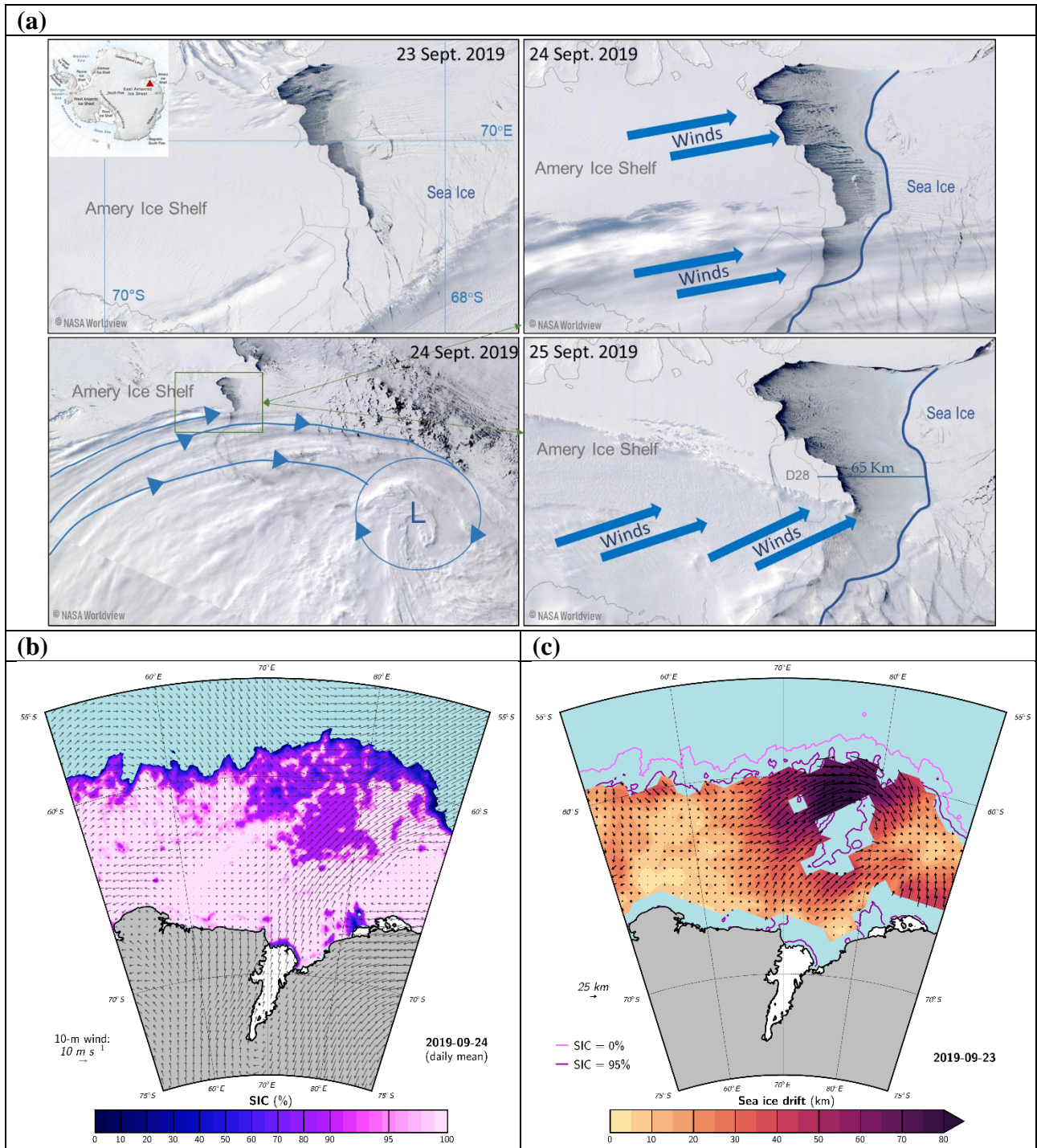


Figure 8: (a) MODIS satellite visible imagery of the Amery Ice Shelf showing the ice shelf before the calving on 23 September 2019, during the calving on 24-25 September 2019. Image credit: NASA Worldview. (b) Satellite-derived sea ice concentrations and ERA5-derived daily mean 10-m winds in vectors over 55-75S and 50-90E on 24 September 2019 at 0000 UTC. (c) Satellite-derived daily sea-ice drift velocity in colors and direction in vectors on 23 September 2019. The solid pink contour is the 0% sea ice concentration contour and the solid purple contour is the 95% sea ice concentration contour.

453 3. Discussion and conclusions

454 In this study, the role of atmospheric extremes in the recent calving of the Amery Ice Shelf in
455 September 2019 is addressed by investigating the atmospheric conditions in combination with the
456 ice and ocean state. During the month of September 2019, the circulation around Antarctica was
457 characterized by anomalously-pronounced 3 ridges and 3 troughs with the Indian sector of the
458 Southern Ocean being under the influence of troughing and surrounded by two blocking ridges;
459 one over the southern Atlantic to the west and one over Davis Sea and southern Australia to the
460 east.

461 During the second half of September 2019, a series of explosive polar cyclones, evolving into
462 stationary twin polar cyclones, impacted the region of the Amery Ice Shelf. The first explosive
463 cyclone occurred on 18 September 2019 and evolved into two stationary twin polar cyclones on
464 19-22 September 2019 sitting to the west of the ice shelf. The second explosive cyclone formed
465 on 23 September 2019 and evolved into two stationary twin polar cyclones on 24-25 September
466 2019, sitting, this time, to the east of the Amery Ice Shelf. Both explosive-cyclone episodes were
467 accompanied by intense atmospheric rivers bringing anomalous warm and moist air masses
468 poleward. The stationary aspect of the deep cyclones had a large impact on the ice conditions as it
469 subjected the ice to sustained stress and strain. The main difference between the two episodes is
470 the location at which the twin cyclones were stationary, relative to the Amery Ice Shelf, which
471 determined the characteristics of the air masses and the wind direction that affected the ice shelf.
472 This position of the cyclones relative to the Amery Ice Shelf was, in turn, determined in each
473 episode, by the location of the blocking ridges in the general circulation.

474 During the first episode, anomalous warm, moist and easterly winds impacted the ice shelf and
475 surrounding sea ice, whereas during the second episode, the ice shelf and surrounding sea ice were
476 under the influence of anomalous westerlies. The first episode resulted in a shoreward storm surge
477 at the front of the ice shelf. During the second episode, anomalously strong offshore winds resulted
478 in an ocean ward slope and an ice-free area in front of the western side of the ice shelf. The
479 sustained strong winds and associated sea surface slope toward the open ocean maintained a strain
480 on the shelf-front and amplified the fracture along the pre-existing rift leading to the calving.

481 The detached iceberg after calving followed a northeasterly motion being dragged by the
482 prevailing winds and associated ocean currents. This drifting direction was similar to the one
483 followed by the sea ice one day before and gave an indication of the impact of the wind direction
484 on this process. Given the east-exposed orientation of the crack at the ice shelf-front, the direction
485 of the sustained strong westerly winds was deterministic for the calving.

486 In summary, atmospheric forcings by the explosive twin polar cyclones induced a gravitationally-
487 driven calving at the Amery Ice Shelf in September 2019 via storm tide and subsequent ocean
488 ward sea-surface slope.

489 The analysis of this unique event could help better understand the underlying factors triggering the
490 calving of ice shelves and hence improve the modelling capabilities of ice shelf future evolution
491 their possible contribution to sea level rise. Our analysis highlights the need for ice sheet models,
492 used to project sea level rise, to account for atmospheric forcing at high resolution, in addition to

493 sea ice and ocean waves, if they were to simulate accurately the changes occurring in the ice sheet
494 and glaciers and their contribution to sea level rise.

495 In fact, important changes in the atmospheric circulation are being observed in the Southern
496 Hemisphere. For instance, between 1979 and 2010 the subtropical jet streams moved poleward by
497 6.5 ± 0.2 degrees in the Southern Hemisphere (Hudson, 2012) and the westerlies strengthened and
498 shifted poleward (Fogt and Marshal, 2020). The observed poleward movement over the past few
499 decades represents a significant change in the position of the sub-tropical jet stream, which should
500 lead to significant latitudinal shifts in the global weather patterns, the hydrological cycle and their
501 impact on Antarctic ice shelves.

502 The variability of the polar jet front in the Southern Hemisphere and whether similar behavior as
503 the polar jet in the Northern Hemisphere is underway around Antarctica needs to be investigated
504 in future work. Several studies have shown evidence for a wavier jet stream in response to rapid
505 Arctic warming and reported a weakening of the polar jet as a result of a reduced temperature
506 gradient between high and mid-latitudes due to the increased temperatures in the Arctic (e.g.,
507 Francis and Vavrus, 2015; Coumou et al., 2015; Mann et al., 2017). Such change in the polar jet,
508 which acts as an isolation boundary between high and mid latitudes, would lead to more
509 interactions, and spark feedback mechanisms between the Antarctic system and mid-latitudes as it
510 happened to be the case in the Arctic (Francis et al., 2018; 2019b).

511 The poleward shift of the cyclones together with the decrease in sea ice extent in recent years
512 makes it more urgent to assess the impact of cyclones on Antarctic-wide maritime-terminating ice
513 shelves as higher numbers of large cyclones could be expected to reach further south and therefore
514 affects ice shelves dynamics. If extreme polar cyclones are to form or reach more frequently ice
515 shelves due to climate change, their destructive effect may have important consequences and needs
516 to be accounted for in models used for sea level and Antarctic Ice Sheet mass balance projections.

517 **4. Data and methods**

518 The atmospheric analysis is based on data from the ERA5 reanalysis (Hersbach et al., 2020).
519 During the period 16-25 September 2019, hourly maps of mean sea level pressure (MSLP), winds,
520 2m temperature and total column water vapor (TCWV) are analyzed. Furthermore, in order to
521 investigate the anomalous character of the atmospheric conditions, we calculated, for the same
522 period and quantities listed above, hourly standardized anomalies and percentile ranks relative to
523 all hourly ERA5 September values during the full record (1979-2019) over the area 45-95°E, 50-
524 75°S. In addition, a histogram analysis has been performed over a smaller domain limited to the
525 ice-shelf front area and adjacent mouth of Prydz Bay (i.e., 70-65°S and 70-75°E). The histograms
526 represent the distribution of hourly values spatially averaged over this domain, for all months
527 during 1979-2019.

528 Daily sea ice extent and concentration data are derived from the AMSR-E / AMSR2 unified record
529 (Meier et al., 2018) at 12.5 km spatial resolution (https://nsidc.org/data/AU_SII2/versions/1). To
530 check the motion in the sea ice field in the Amery Basin, we used the low-resolution sea ice drift
531 product of the EUMETSAT Ocean and Sea Ice Satellite Application Facility (OSI SAF, www.osi-saf.org). This is a 48-hour average gridded ice drift dataset processed on a daily basis and made
532

533 available on a 62.5 km Polar Stereographic Grid (e.g., Kwok et al. 2017). Ice motion vectors are
534 estimated by an advanced cross-correlation method on pairs of satellite images (Lavergne et al.,
535 2010). It uses the multi-sensor spatial covering product that combines SSMIS (91 GHz H and V
536 polarization) on board DMSP platform F17, ASCAT (C-band backscatter) on board EUMETSAT
537 platform Metop-A, and AMSR-2 on board JAXA platform GCOM-W. Due to atmospheric noise
538 and surface melting these data are only available for the Southern Hemisphere winter (1st April to
539 31st October).

540 Visible imagery of the Amery Ice Shelf and surrounding area are taken from MODIS/VIIRS land
541 products (ORNL DAAC, 2018) using the NASA Worldview application
542 (<https://worldview.earthdata.nasa.gov>).

543 Sentinel-1 data has been used to determine potential surface melt (e.g., Datta et. al, 2019) and to
544 track ice velocity over the Amery ice shelf prior to the D28 iceberg calving by using feature
545 tracking in ESA’s SNAP Sentinel-1 toolbox. Sentinel-3A and 3B data were used via the ESA
546 Ocean Virtual Laboratory application to determine the wave height at the front of the Amery Ice
547 Shelf.

548 The ocean slope and elevation are taken from the Hybrid Coordinate Ocean Model (HYCOM,
549 <https://www.hycom.org/>). HYCOM (Cummings and Smedstad, 2013) is a data-assimilative hybrid
550 isopycnal-sigma-pressure (generalized) coordinate ocean model of which we downloaded
551 elevation from the Google Earth Engine at 0.08-degree latitude/longitude grid. Based on this
552 elevation dataset, the surface slope was derived as the local gradient using the 4-connected
553 neighbors of each pixel.

554 **Acknowledgments**

555 We acknowledge the use of imagery from the NASA Worldview application
556 (<https://worldview.earthdata.nasa.gov>), part of the NASA Earth Observing System Data and
557 Information System (EOSDIS). This work was supported by Masdar Abu Dhabi Future Energy
558 Company, United Arab Emirates, Grant 8434000221. The contribution of Petra Heil was supported
559 by the Australian Government’s Australian Antarctic Partnership Program, and contributes to AAS
560 Project 4506.

561 **Code and Data availability:** All data needed to evaluate the conclusions in the paper are present
562 in the paper. Correspondence and requests for materials should be addressed to DF.

563 **Author contributions** D.F. conceived the study and wrote the initial manuscript. K.M. analyzed
564 the satellite and reanalysis data. S.L analyzed satellite data. M.T. and P.H. provided input on result
565 analysis. All authors interpreted results and provided input to the final manuscript.

566 **Competing Interests** The authors declare that they have no competing interests.

567 **References**

568 1. Allen, J.T., Pezza, A. B., and Black, M. T. (2010) Explosive cyclogenesis: a global climatology
569 comparing multiple reanalyses. *Journal of Climate*, v.23, 6468–6484.

570 2. Aitken, A., Roberts, J., Ommen, T. et al. Repeated large-scale retreat and advance of Totten
571 Glacier indicated by inland bed erosion. *Nature* 533, 385–389 (2016).
572 <https://doi.org/10.1038/nature17447>.

573 3. Barnes, E. A., and L. Polvani (2013), Response of the midlatitude jets, and of their variability,
574 to increased greenhouse gases in the CMIP5 Models, *J. Clim.*, 26, 7117– 7135.

575 4. Bassis, J., Fricker, H., Coleman, R., & Minster, J. (2008). An investigation into the forces that
576 drive ice-shelf rift propagation on the Amery Ice Shelf, East Antarctica. *Journal of Glaciology*,
577 54(184), 17-27. doi:10.3189/002214308784409116.

578 5. Bassis, J. N. and Ma, Y.: Evolution of basal crevasses links ice shelf stability to ocean forcing,
579 *Earth Planet. Sci. Lett.*, 409, 203–211, <https://doi.org/10.1016/j.epsl.2014.11.003>, 2015.

580 6. Bengtsson, L., K. I. Hodges, and N. Keenlyside (2009), Will extratropical storms intensify in
581 a warmer climate? *J. Clim.*, 22(9), 2276– 2301.

582 7. Benn D. I. and J. A. Åström (2018) Calving glaciers and ice shelves, *Advances in Physics: X*,
583 3:1, DOI: 10.1080/23746149.2018.1513819.

584 8. Bromirski, P. D., Sergienko, O. V. & MacAyeal, D. R. Transoceanic infragravity waves
585 impacting Antarctic ice shelves. *Geophys. Res. Lett.* 37, L02502 (2010).

586 ~~8.~~9. Brunt, K., Okal, E., & MacAyeal, D. (2011). Antarctic ice-shelf calving triggered by the
587 Honshu (Japan) earthquake and tsunami, March 2011. *Journal of Glaciology*, 57(205), 785-
588 788. doi:10.3189/002214311798043681.

589 ~~9.~~10. Chang, E. K. M., Y. Guo, and X. Xia (2012), CMIP5 multimodel ensemble projection of
590 storm track change under global warming, *J. Geophys. Res.*, 117, D23118,
591 doi:10.1029/2012JD018578.

592 ~~10.~~11. Chang, E. K. M., 2017: Projected Significant Increase in the Number of Extreme
593 Extratropical Cyclones in the Southern Hemisphere. *J. Climate*, 30, 4915–4935,
594 <https://doi.org/10.1175/JCLI-D-16-0553.1>.

595 ~~11.~~12. Cook, A. J. and Vaughan, D. G.: Overview of areal changes of the ice shelves on the
596 Antarctic Peninsula over the past 50 years, *The Cryosphere*, 4, 77–98,
597 <https://doi.org/10.5194/tc-4-77-2010>, 2010.

598 ~~12.~~13. Coumou D., J. Lehmann, J. Beckmann, (2015), The weakening summer circulation in the
599 Northern Hemisphere mid-latitudes, *Science*, Vol. 348, Issue 6232, pp. 324-327. DOI:
600 10.1126/science.1261768.

601 ~~13.~~14. Cummings, J.A. and O.M. Smedstad, 2013: Variational data analysis for the global ocean.
602 In: S.K. Park and L. Xu (Eds.), *Data Assimilation for Atmospheric, Oceanic and Hydrologic*
603 Applications Vol. II., DOI 10.1007/978-3-642-35088-7_13, Springer-Verlag Berlin
604 Heidelberg.

605 ~~14.~~15. Datta, R. T. Tedesco, M., Fettweis, X., Agosta, C., Lhermitte, S., Lenaerts, J.T.M., Wever,
606 N. (2019) The Effect of Foehn-Induced Surface Melt on Firn Evolution Over the Northeast
607 Antarctic Peninsula. *Geophys. Res. Lett.* 46, 3822–383, doi: 10.1029/2018GL080845.

608 ~~15.~~16. Davies, H. C., 1997: Emergence of the mainstream cyclogenesis theories. *Meteor. Z.*,6,
609 261–274.

610 ~~16~~.17. DeConto, R., Pollard, D. Contribution of Antarctica to past and future sea-level rise. *Nature*
611 531, 591–597 (2016), <https://doi.org/10.1038/nature17145>.

612 18. Dolatshah, A., Nelli, F., Alberello, A., Bruneau, L., Bennetts, L. G., Meylan, M. H., Monty, J.
613 P., and Toffoli, A. "Wave Attenuation due to Ice Cover: An Experimental Model in a Wave-
614 Ice Flume." *Proceedings of the ASME 2017 36th International Conference on Ocean, Offshore*
615 *and Arctic Engineering*. Volume 8: Polar and Arctic Sciences and Technology; Petroleum
616 Technology. Trondheim, Norway. June 25–30, 2017. V008T07A016. ASME.
617 <https://doi.org/10.1115/OMAE2017-61548>.

618 ~~17~~.19. Darji S., S.R. Oza, R. D. Shah, B. P. Rathore and I. M. Bahuguna, 2018: *Rift assessment*
619 *and potential calving zone of Amery Ice Shelf, East Antarctica*. *Current Science*, 115, 1799-
620 1804, doi: 10.18520/cs/v115/i9/1799-1804.

621 ~~18~~.20. Eayrs, C., Holland, D. M., Francis, D., Wagner, T. J. W., Kumar, R., & Li, X. (-2019).
622 Understanding the seasonal cycle of Antarctic sea ice extent in the context of longer-term
623 variability. *Reviews of Geophysics*. 57, 1037– 1064, <https://doi.org/10.1029/2018RG000631>.

624 ~~19~~.21. Ferreira, R. N., W. N.Schubert, and J. J.Hack, 1996: Dynamical aspects of twin tropical
625 cyclones associated with the Madden–Julian oscillation.*J. Atmos. Sci.*, 53, 929–945.

626 ~~20~~.22. Francis J. A. and S. J. Vavrus, 2015, Evidence for a wavier jet stream in response to rapid
627 Arctic warming, *Environ. Res. Lett.* 10 014005.

628 ~~21~~.23. Francis D., C. Eayrs, J-P. Chaboureau, T. Mote, D. Holland (2018), "Polar jet associated
629 circulation triggered a Saharan cyclone and derived the poleward transport of the African dust
630 generated by the cyclone" *Journal of Geophysical Research: Atmospheres*.
631 DOI:10.1029/2018JD029095.

632 ~~22~~.24. Francis D., C. Eayrs, J. Cuesta, D. Holland (2019a), Polar cyclones at the origin of the
633 reoccurrence of the Maud Rise Polynya in austral winter 2017, *Journal of Geophysical*
634 *Research: Atmospheres*,124. <https://doi.org/10.1029/2019JD030618>, 2019.

635 ~~23~~.25. Francis D., C. Eayrs, J-P. Chaboureau, T. Mote, D. Holland (2019b), A meandering polar
636 jet caused the development of a Saharan cyclone and the transport of dust toward Greenland,
637 *Adv. Sci. Res.*, 1, 1–8, <https://doi.org/10.5194/asr-16-49-2019>, 2019.

638 ~~24~~.26. Francis D., K.S. Mattingly, N. Alshamsi, M. Temimi, R. Massom, P. Heil, 2020, On the
639 crucial role of atmospheric rivers in the two major Weddell Polynya events in 1973 and 2017
640 in Antarctica. *Sci. Adv.* 6, eabc2695 (2020).
641 <https://advances.sciencemag.org/content/6/46/eabc2695>.

642 ~~25~~.27. Fricker, H., Young, N., Allison, I., & Coleman, R. (2002). Iceberg calving from the Amery
643 Ice Shelf, East Antarctica. *Annals of Glaciology*, 34, 241-246.
644 doi:10.3189/172756402781817581

645 ~~26~~.28. Fricker, H. A., N. W. Young, R. Coleman, J. N. Bassis, and J.-B. Minster (2005), Multi-
646 year monitoring of rift propagation on the Amery Ice Shelf, East Antarctica, *Geophys. Res.*
647 *Lett.*, 32, L02502, doi:10.1029/2004GL021036.

648 ~~27~~.29. Fogt, RL, Marshall, GJ. The Southern Annular Mode: Variability, trends, and climate
649 impacts across the Southern Hemisphere. *WIREs Clim Change*. 2020; 11:e652.
650 <https://doi.org/10.1002/wcc.652>

651 ~~28~~.30. Fyfe, J. C. (2003), Extratropical Southern Hemisphere cyclones: Harbingers of climate
652 change?, *J. Clim.*, 16, 2802– 2805.

653 ~~29.~~31. Galton-Fenzi, B. K., J. R. Hunter, R. Coleman, S. J. Marsland, and R. C. Warner (2012),
654 Modeling the basal melting and marine ice accretion of the Amery Ice Shelf, *J. Geophys. Res.*,
655 117, C09031, doi:10.1029/2012JC008214.

656 ~~30.~~32. Greenbaum, J., Blankenship, D., Young, D. et al. Ocean access to a cavity beneath Totten
657 Glacier in East Antarctica. *Nature Geosci* 8, 294–298 (2015).
658 <https://doi.org/10.1038/ngeo2388>.

659 ~~31.~~33. Grieger J., G. C. Leckebusch, C. C. Raible, I. Rudeva & I. Simmonds (2018) Subantarctic
660 cyclones identified by 14 tracking methods, and their role for moisture transports into the
661 continent, *Tellus A: Dynamic Meteorology and Oceanography*, 70:1, 1-18, DOI:
662 10.1080/16000870.2018.1454808.

663 ~~32.~~34. Hersbach, H., B. Bell, P. Berrisford, et al., 2020: The ERA5 global reanalysis. *Quarterly*
664 *Journal of the Royal Meteorological Society*, 146, 1999–2049, doi: 10.1002/qj.3803. Hogg, A.,
665 Gudmundsson, G. Impacts of the Larsen-C Ice Shelf calving event. *Nature Clim Change* 7,
666 540–542 (2017). <https://doi.org/10.1038/nclimate3359>.

667 ~~33.~~35. Holdsworth, G. & Glynn, J. Iceberg calving from floating glaciers by a vibration
668 mechanism. *Nature* 274, 464–466 (1978).

669 36. Hudson, R. D.: Measurements of the movement of the jet streams at mid-latitudes, in the
670 Northern and Southern Hemispheres, 1979 to 2010, *Atmos. Chem. Phys.*, 12, 7797–7808,
671 <https://doi.org/10.5194/acp-12-7797-2012>, 2012.

672 ~~34.~~37. Irving, D., & Simmonds, I. (2015). A Novel Approach to Diagnosing Southern Hemisphere
673 Planetary Wave Activity and Its Influence on Regional Climate Variability, *Journal of Climate*,
674 28(23), 9041-9057. Retrieved Jan 28, 2021, from
675 <https://journals.ametsoc.org/view/journals/clim/28/23/jcli-d-15-0287.1.xml>.

676 ~~35.~~38. Jeong, S., I. M. Howat, and J. N. Bassis (2016), Accelerated ice shelf rifting and retreat at
677 Pine Island Glacier, West Antarctica, *Geophys. Res. Lett.*, 43, 11,720–11,725,
678 doi:10.1002/2016GL071360.

679 ~~36.~~39. King, M. A., R. Coleman, A.-J. Freemantle, H. A. Fricker, R. S. Hurd, B. Legrésy, L.
680 Padman, and R. Warner (2009), A 4-decade record of elevation change of the Amery Ice Shelf,
681 East Antarctica, *J. Geophys. Res.*, 114, F01010, doi:10.1029/2008JF001094.

682 ~~37.~~40. Kohout, A., Williams, M., Dean, S. et al. Storm-induced sea-ice breakup and the
683 implications for ice extent. *Nature* 509, 604–607 (2014). <https://doi.org/10.1038/nature13262>

684 ~~38.~~41. ~~Kossin P.J., K.R. Knapp, T.L. Olander, C.S. Velden, 2020, Global increase in major~~
685 ~~tropical cyclone exceedance probability over the past four decades, *Proceedings of the National*~~
686 ~~*Academy of Sciences* May 2020, 201920849; DOI: 10.1073/pnas.1920849117.~~

687 ~~39.~~42. Kwok, R., Pang, S. S., and Kacimi, S.: Sea ice drift in the Southern Ocean: Regional
688 patterns, variability and trends, *Elem. Sci. Anth.*, 5, 1–16,
689 <https://doi.org/10.1525/elementa.226>, 2017.

690 ~~40.~~43. Lambert, S. J., and J. C. Fyfe (2006), Changes in winter cyclone frequencies and strengths
691 simulated in enhanced greenhouse warming experiments: Results from the models
692 participating in the IPCC diagnostic exercise, *Clim. Dyn.*, 26, 713–728.

693 44. Lavergne, T., Eastwood, S., Teffah, Z., Schyberg, H., and Breivik, L.-A. (2010), Sea ice
694 motion from low-resolution satellite sensors: An alternative method and its validation in the
695 Arctic, *J. Geophys. Res.*, 115, C10032, doi:10.1029/2009JC005958.

696 41-45. Lee, S., Gong, T., Feldstein, S. B., Screen, J. A., & Simmonds, I. (2017). Revisiting the
697 cause of the 1989–2009 Arctic surface warming using the surface energy budget: Downward
698 infrared radiation dominates the surface fluxes. *Geophysical Research Letters*, 44, 10,654–
699 10,661. <https://doi.org/10.1002/2017GL075375>.

700 42-46. Lim, Eun-Pa; Simmonds, Ian (2002). Explosive Cyclone Development in the Southern
701 Hemisphere and a Comparison with Northern Hemisphere Events. *Monthly Weather Review*.
702 130 (9): 2188–2209. Bibcode:2002 MWRv. .130.2188L. doi:10.1175/1520-
703 0493(2002)130<2188:ECDITS>2.0.CO;2.

704 43-47. Liu Y., J. C. Moore, X. Cheng, R. M. Gladstone, J. N. Bassis, H. Liu, J. Wen, F. Hui, 2015,
705 Iceberg calving of Antarctic ice shelves, *Proceedings of the National Academy of Sciences*,
706 March 2015, 112 (11) 3263-3268; DOI: 10.1073/pnas.1415137112.

707 44-48. Mann, M., Rahmstorf, S., Kornhuber, K. et al. Influence of Anthropogenic Climate Change
708 on Planetary Wave Resonance and Extreme Weather Events. *Sci Rep* 7, 45242 (2017).
709 <https://doi.org/10.1038/srep45242>

710 45-49. Massom, R.A., Scambos, T.A., Bennetts, L.G. et al. Antarctic ice shelf disintegration
711 triggered by sea ice loss and ocean swell. *Nature* 558, 383–389 (2018).
712 <https://doi.org/10.1038/s41586-018-0212-1>.

713 46-50. Matear, R., O’Kane, T., Risbey, J. et al. Sources of heterogeneous variability and trends in
714 Antarctic sea-ice. *Nat Commun* 6, 8656 (2015). <https://doi.org/10.1038/ncomms9656>.

715 47-51. Meier, W. N., T. Markus, and J. C. Comiso. 2018. AMSR-E/AMSR2 Unified L3 Daily
716 12.5 km Brightness Temperatures, Sea Ice Concentration, Motion & Snow Depth Polar Grids,
717 Version 1. [Antarctica]. Boulder, Colorado USA. NASA National Snow and Ice Data Center
718 Distributed Active Archive Center. doi: <https://doi.org/10.5067/RA1MIJOYPK3P> [10 April
719 2020].

720 48-52. Morrison K.A., A. M. Hogg, M.H. England and P. Spence Warm Circumpolar Deep Water
721 transport toward Antarctica driven by local dense water export in canyons, *Science Advances*,
722 2020: Vol. 6, no. 18, eaav2516, DOI: 10.1126/sciadv.aav2516.

723 53. Moustauoui, M., H. Teitelbaum, C. Basdevant, and Y. Boughaleb, Linked behavior of twin
724 tropical cyclones, *J. Geophys. Res.*, 107(D19), 4378, doi:10.1029/2000JD000066, 2002.

725 49-54. Neu, U., Akperov, M. G., Bellenbaum, N., Benestad, R., Blender, R., Caballero, R.,
726 Cocozza, A., Dacre, H. F., Feng, Y., Fraedrich, K., Grieger, J., Gulev, S., Hanley, J., Hewson,
727 T., Inatsu, M., Keay, K., Kew, S. F., Kindem, I., Leckebusch, G. C., Liberato, M. L. R.,
728 Lionello, P., Mokhov, I. I., Pinto, J. G., Raible, C. C., Reale, M., Rudeva, I., Schuster, M.,
729 Simmonds, I., Sinclair, M., Sprenger, M., Tilinina, N. D., Trigo, I. F., Ulbrich, S., Ulbrich, U.,
730 Wang, X. L., & Wernli, H. (2013). IMILAST: A Community Effort to Intercompare
731 Extratropical Cyclone Detection and Tracking Algorithms, *Bulletin of the American*
732 *Meteorological Society*, 94(4), 529-547. Retrieved Jan 28, 2021, from
733 <https://journals.ametsoc.org/view/journals/bams/94/4/bams-d-11-00154.1.xml>.

734 55. ORNL DAAC. 2018. MODIS and VIIRS Land Products Global Subsetting and Visualization
735 Tool. ORNL DAAC, Oak Ridge, Tennessee, USA. Accessed May 20, 2020. Subset obtained
736 for MOD13Q1 product over the Amery Ice Shelf – Antarctica, time period: 2019-09-01 to
737 2019-09-30. <https://doi.org/10.3334/ORNLDAAC/1379>.

738 ~~50.~~56. Pezza, A.B., Simmonds, I. and Renwick, J.A. (2007), Southern hemisphere cyclones and
739 anticyclones: recent trends and links with decadal variability in the Pacific Ocean. *Int. J.*
740 *Climatol.*, 27: 1403-1419. <https://doi.org/10.1002/joc.1477>.

741 ~~51.~~57. Pope, J. O., Holland, P. R., Orr, A., Marshall, G. J., and Phillips, T. (2017), The impacts
742 of El Niño on the observed sea ice budget of West Antarctica, *Geophys. Res. Lett.*, 44, 6200–
743 6208, doi:10.1002/2017GL073414.

744 ~~52.~~58. Pritchard, H. D., Ligtenberg S.R., Fricker H.A., Vaughan D.G., van den Broeke MR,
745 Padman L., Antarctic ice-sheet loss driven by basal melting of ice shelves. *Nature* 484, 502–
746 505 (2012).

747 ~~53.~~59. Reale M., M. L.R. Liberato, P. Lionello, J. G. Pinto, S. Salon & S. Ulbrich (2019) A Global
748 Climatology of Explosive Cyclones using a Multi-Tracking Approach, *Tellus A: Dynamic*
749 *Meteorology and Oceanography*, 71:1, DOI: 10.1080/16000870.2019.1611340.

750 ~~54.~~60. Raphael, M. N., 2007, The influence of atmospheric zonal wave three on Antarctic sea ice
751 variability, *J. Geophys. Res.*, 112, D12112, <https://doi.org/10.1029/2006JD007852>, 2007.

752 ~~55.~~61. Renfrew A.I., G.W.K. Moore and A.A. Clerk (1997) Binary interactions between polar
753 lows, *Tellus A: Dynamic Meteorology and Oceanography*, 49:5, 577-594, DOI:
754 10.3402/tellusa.v49i5.14823.

755 ~~56.~~62. Rignot, E. et al. Accelerated ice discharge from the Antarctic Peninsula following the
756 collapse of Larsen B ice shelf. *Geophys. Res. Lett.* 31, <https://doi.org/10.1029/2004gl020697>
757 (2004).

758 ~~57.~~63. Rignot E., J. Mouginot, B. Scheuchl, M. van den Broeke, M. J. van Wessem, M.
759 Morlighem, 2019, Four decades of Antarctic Ice Sheet mass balance from 1979–2017,
760 *Proceedings of the National Academy of Sciences* Jan 2019, 116 (4) 1095-1103; DOI:
761 10.1073/pnas.1812883116.

762 ~~58.~~64. Robinson, W. & Haskell, T. G. Calving of Erebus Glacier tongue. *Nature* 346, 615–616
763 (1990).

764 65. Robinson, W. & Haskell, T. G. Travelling flexural waves in the Erebus Glacier Tongue,
765 McMurdo Sound, Antarctica. *Cold Reg. Sci. Technol.* 20, 289–293 (1992).

766 ~~59.~~66. Rudeva I., I. Simmonds, Variability and trends of global atmospheric frontal activity and
767 links with large-scale modes of variability. *J. Climate* 28, 3311–3330 (2015).

768 ~~60.~~67. Sanders, Frederick; Gyakum, John R (1980). "Synoptic-Dynamic Climatology of the
769 'Bomb'. *Monthly Weather Review.* 108 (10): 1589–606. Bibcode:1980 MWRv.108.1589S.
770 doi:10.1175/1520-0493(1980)108<1589:SDCOT>2.0.CO;2.

771 68. Scambos, T. A., Bohlander, J. A., Shuman, C. A. & Skvarca, P. Glacier acceleration and
772 thinning after ice shelf collapse in the Larsen B embayment, Antarctica. *Geophys. Res. Lett.*
773 31,1 –4 (2004).

774 69. Scambos, T., Ross, R., Bauer, R., Yermolin, Y., Skvarca, P., Long, D., Bohlander, J. and
775 Haran, T., 2008. Calving and ice-shelf break-up processes investigated by proxy: Antarctic
776 tabular iceberg evolution during northward drift. *Journal of Glaciology*, 54(187), pp.579-591.

777 ~~61.~~70. Scambos, T. A., Berthier, E., Haran, T., Shuman, C. A., Cook, A. J., Ligtenberg, S. R. M.,
778 and Bohlander, J.: Detailed ice loss pattern in the northern Antarctic Peninsula: widespread
779 decline driven by ice front retreats, *The Cryosphere*, 8, 2135–2145, [https://doi.org/10.5194/tc-](https://doi.org/10.5194/tc-8-2135-2014)
780 8-2135-2014, 2014.

781 ~~62~~.71. Schemm, S. (2018), Regional trends in weather systems help explain Antarctic sea ice
782 trends. *Geophysical Research Letters*, 45, 7165–7175. <https://doi.org/10.1029/2018GL079109>.

783 ~~63~~.72. Schlosser E., J.G. Powers, M.G. Duda, K.W. Manning (2011) Interaction between
784 Antarctic sea ice and synoptic activity in the circumpolar trough: implications for ice-core
785 interpretation, *Annals of Glaciology* 52(57) 2011.

786 ~~64~~.73. Schlosser E., F. A. Haumann, M. N. Raphael Atmospheric influences on the anomalous
787 2016 Antarctic sea ice decay (2018), *The Cryosphere*, 12, 1103–1119, 2018,
788 <https://doi.org/10.5194/tc-12-1103-2018>.

789 ~~65~~.74. Schosler, V., Aquino, F.E., Reis, P.A. et al. Antarctic atmospheric circulation anomalies
790 and explosive cyclogenesis in the spring of 2016. *Theor Appl Climatol* (2020).
791 <https://doi.org/10.1007/s00704-020-03200-9>.

792 ~~66~~.75. Shepherd, A., Fricker, H. A. & Farrell, S. L. Trends and connections across the Antarctic
793 cryosphere. *Nature* 558, 223–232 (2018).

794 ~~67~~.76. Shimada, U., A. Wada, K. Yamazaki, N. Kitabatake (2014) Roles of an upper-level cold
795 vortex and low-level baroclinicity in the development of polar lows over the Sea of Japan,
796 *Tellus A: Dynamic Meteorology and Oceanography*, 66:1, DOI: 10.3402/tellusa.v66.24694.

797 ~~68~~.77. Smith, J.A., Graham, A.G.C., Post, A.L. et al. The marine geological imprint of Antarctic
798 ice shelves. *Nat Commun* 10, 5635 (2019). <https://doi.org/10.1038/s41467-019-13496-5>.

799 ~~69~~.78. Son, S.-W., L. M. Polvani, D. W. Waugh, H. Akiyoshi, R. Garcia, D. Kinnison, S. Pawson,
800 E. Rozanov, T. G. Shepherd, and K. Shibata (2008), The impact of stratospheric ozone
801 recovery on the Southern Hemisphere westerly jet, *Science*, 320, 1486–1489.

802 ~~70~~.79. Squire, V. A., Robinson, W. H., Meylan, M. H. & Haskell, T. G. Observations of flexural
803 waves in the Erebus Glacier Tongue, McMurdo Sound, Antarctica, and nearby sea ice. *J.*
804 *Glaciol.* 40, 377–385 (1994).

805 ~~71~~.80. Stoll P.J., Graverson RG., Noer G, Hodges K. An objective global climatology of polar
806 lows based on reanalysis data. *QJRMeteorol.Soc.*2018;144:2099–2117.
807 <https://doi.org/10.1002/qj.3309>

808 ~~72~~.81. Swart S., E. C. Cambell, C. H. Heuze, K. Johnson, J. L. Lieser, R. Masson, M. Mazloff,
809 M. Meredith, P. Reid, J.-B. Sallee, S. Stammerjohn (2018) Litmus or sea ice anomaly? Sidebar,
810 *State of the Climate, BAMS*, August 2018, DOI:10.1175/BAMS-D-18-0173.1.

811 ~~82~~. Tamarin, T., and Y. Kaspi (2017), The poleward shift of storm tracks under global warming:
812 A Lagrangian perspective, *Geophys. Res. Lett.*, 44, 10,666–10,674,
813 [doi:10.1002/2017GL073633](https://doi.org/10.1002/2017GL073633).

814 ~~73~~.83. Li T., Y. Liu and X. Cheng, 2020: Recent and imminent calving events do little to impair
815 Amery ice shelf's stability. *Acta Oceanologica Sinica*, 39, 168-170, doi: 10.1007/s13131-020-
816 1600-6.

817 ~~74~~.84. Turner J., S.A. Harangozo, G.J. Marshall, J.C. King, S.R. Colwell (2002) Anomalous
818 atmospheric circulation over the Weddell Sea, Antarctica during the Austral summer of
819 2001/02 resulting in extreme sea ice conditions, *Geophys.Res. Lett.*, Vol. 29, N0. 24, 2160,
820 [doi:10.1029/2002GL015565](https://doi.org/10.1029/2002GL015565), 2002.

821 ~~85~~. Uccellini L.W. (1990) Processes Contributing to the Rapid Development of Extratropical
822 Cyclones. In: Newton C.W., Holopainen E.O. (eds) *Extratropical Cyclones*. American
823 Meteorological Society, Boston, MA.

824 ~~75.~~86. Ulbrich, U., Leckebusch, G. C., Grieger, J., Schuster, M., Akperov, M., Bardin, M. Y.,
825 Feng, Y., Gulev, S., Inatsu, M., Keay, K., Kew, S. F., Liberato, M. L. R., Lionello, P., Mokhov,
826 I. I., Neu, U., Pinto, J. G., Raible, C. C., Reale, M., Rudeva, I., Simmonds, I., Tilinina, N. D.,
827 Trigo, I. F., Ulbrich, S., Wang, X. L. and Wernli, H. (2013) Are greenhouse gas signals of
828 Northern Hemisphere winter extra-tropical cyclone activity dependent on the identification and
829 tracking algorithm? *Meteorologische Zeitschrift*, 22 (1). pp. 61-68. ISSN 0941-2948. doi:
830 <https://doi.org/10.1127/0941-2948/2013/0420>.

831 ~~76.~~87. Uotila, P., T. Vihma, A. B. Pezza, I. Simmonds, K. Keay, and A. H. Lynch (2011),
832 Relationships between Antarctic cyclones and surface conditions as derived from high-
833 resolution numerical weather prediction data, *J. Geophys. Res.*, 116, D07109,
834 [doi:10.1029/2010JD015358](https://doi.org/10.1029/2010JD015358).

835 88. Vaughan, D. G., H. F. J. Corr, R. A. Bindschadler, P. Dutrieux, G. H. Gudmundsson, A.
836 Jenkins, T. Newman, P. Vornberger, and D. J. Wingham (2012), Subglacial melt channels and
837 fracture in the floating part of Pine Island Glacier, Antarctica, *J. Geophys. Res.*, 117, F03012,
838 [doi:10.1029/2012JF002360](https://doi.org/10.1029/2012JF002360).

839 ~~77.~~89. Vernon A. Squire, 2020: Ocean wave interactions with sea ice: A reappraisal. *Annual*
840 Review of Fluid Mechanics, 52, 37-60, doi: [10.1146/annurev-fluid-010719-060301](https://doi.org/10.1146/annurev-fluid-010719-060301).

841 ~~78.~~90. Vichi, M., Eayrs, C., Alberello, A., Bekker, A., Bennetts, L., Holland, D., et al. (2019).
842 Effects of an explosive polar cyclone crossing the Antarctic marginal ice zone. *Geophysical*
843 *Research Letters*, 46, 5948–5958. <https://doi.org/10.1029/2019GL082457>.

844 ~~79.~~91. Wagner J.S., A. Gohm, A. Dörnbrack, A. Schäfler (2011), The mesoscale structure of a
845 polar low: airborne lidar measurements and simulations. *Q. J. R. Meteorol. Soc.* DOI:
846 [10.1002/qj.857](https://doi.org/10.1002/qj.857).

847 ~~80.~~92. Watanabe, S. I., and H. Niino, 2014: Genesis and Development Mechanisms of a Polar
848 Mesocyclone over the Japan Sea. *Mon. Wea. Rev.*, 142, 2248–2270,
849 <https://doi.org/10.1175/MWR-D-13-00226.1>.

850 ~~81.~~93. Wei, L., Qin, T. Characteristics of cyclone climatology and variability in the Southern
851 Ocean. *Acta Oceanol. Sin.* 35, 59–67 (2016). <https://doi.org/10.1007/s13131-016-0913-y>.

852 ~~82.~~94. Wille, J. D., V. Favier, A. Dufour, I. V. Gorodetskaya, J. Turner, C. Agosta and F. Codron,
853 2019: West Antarctic surface melt triggered by atmospheric rivers. *Nature Geoscience*, 12,
854 911-916, doi: [10.1038/s41561-019-0460-1](https://doi.org/10.1038/s41561-019-0460-1).

855 ~~83.~~95. Woods, C., and R. Caballero, 2016: The Role of Moist Intrusions in Winter Arctic
856 Warming and Sea Ice Decline. *J. Climate*, 29, 4473–4485, [https://doi.org/10.1175/JCLI-D-15-](https://doi.org/10.1175/JCLI-D-15-0773.1)
857 [0773.1](https://doi.org/10.1175/JCLI-D-15-0773.1).

858 ~~84.~~96. Yokoyama, Y.; Yamamoto, M., 2019, Influences of surface heat flux on twin cyclone
859 structure during their explosive development over the East Asian marginal seas on 23 January
860 2008. *Weather Clim. Extrem.* 2019, 23, 100198. <https://doi.org/10.1016/j.wace.2019.100198>.

861 ~~85.~~97. Zhao, C., Cheng, X., Liu, Y., Hui, F., Kang, J., Wang, X., Cheng, C. (2013). The slow-
862 growing tooth of the Amery Ice Shelf from 2004 to 2012. *Journal of Glaciology*, 59(215), 592-
863 596. doi:10.3189/2013JoG12J225.